



Master Thesis

Surface study of polymer solutions by optical method under intense electric field

Study programme:

N0723A270002 Textile Engineering

Author:

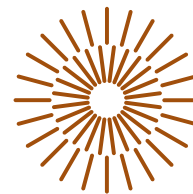
Astha Vishwakarma

Thesis Supervisors:

doc. Ing. Pavel Pokorný, Ph.D.

Department of Nonwovens and Nanofibrous materials

Liberec 2023



Master Thesis Assignment Form

Surface study of polymer solutions by optical method under intense electric field

Name and surname: **Astha Vishwakarma**
Identification number: T21000312
Study programme: N0723A270002 Textile Engineering
Assigning department: Department of Nonwovens and Nanofibrous materials
Academic year: 2022/2023

Rules for Elaboration:

1. Literature review on visualizing surface waves of the polymer solution.
2. Design of experiment and equipment development based on the secondary research findings.
3. Implement the designed experiment to produce the results.
4. Discuss the obtained results and propose hypotheses and recommend solutions.

Scope of Graphic Work:

Scope of Report: 40-60

Thesis Form: printed/electronic

Thesis Language: english

List of Specialised Literature:

1. Lukas, D., Sarkar, A., & Pokorny, P. (2008). Self-organization of jets in electrospinning from free liquid surface: A generalized approach. *Journal of Applied Physics* 103, 084309 (2008).
2. Måløy, K., Feder, J., & Jo/ssang, T. (1989). An experimental technique for measurements of capillary waves. *Rev Sci Instrum* 60, 481-486 (1989).
3. Shmyrov, A., Mizev, A., Shmyrova, A., & Mizeva, I. (2019). Capillary wave method: An alternative approach to wave excitation and to wave profile reconstruction. *Physics of Fluids* 31, 012101 (2019).
4. Zeleny, J. (1914). The Electrical Discharge from Liquid Points, and a Hydrostatic Method of Measuring the Electric Intensity at Their Surfaces. *Physical review journals archive (American Physical Society)*.

Thesis Supervisors: doc. Ing. Pavel Pokorný, Ph.D.
Department of Nonwovens and Nanofibrous
materials

Date of Thesis Assignment: November 1, 2022

Date of Thesis Submission: June 2, 2023

L.S.

doc. Ing. Vladimír Bajzík, Ph.D.
Dean

doc. Ing. Jiří Chvojka, Ph.D.
Head of Department

Liberec November 1, 2022

Declaration

I hereby certify, I, myself, have written my master thesis as an original and primary work using the literature listed below and consulting it with my thesis supervisor and my thesis counsellor.

I acknowledge that my master thesis is fully governed by Act No. 121/2000 Coll., the Copyright Act, in particular Article 60 – School Work.

I acknowledge that the Technical University of Liberec does not infringe my copyrights by using my master thesis for internal purposes of the Technical University of Liberec.

I am aware of my obligation to inform the Technical University of Liberec on having used or granted license to use the results of my master thesis; in such a case the Technical University of Liberec may require reimbursement of the costs incurred for creating the result up to their actual amount.

At the same time, I honestly declare that the text of the printed version of my master thesis is identical with the text of the electronic version uploaded into the IS/STAG.

I acknowledge that the Technical University of Liberec will make my master thesis public in accordance with paragraph 47b of Act No. 111/1998 Coll., on Higher Education Institutions and on Amendment to Other Acts (the Higher Education Act), as amended.

I am aware of the consequences which may under the Higher Education Act result from a breach of this declaration.

June 2, 2023

Astha Vishwakarma

Acknowledgement

I am sincerely grateful to Doc. Pavel Pokorný for his exceptional supervision, support, and encouragement throughout this project. His guidance was instrumental in the successful completion of this endeavor, and I am deeply thankful for the opportunity to explore this captivating realm of scientific exploration. My appreciation also extends to those who provided the necessary literature and assisted in the laboratory, as their contributions were invaluable to the progress and achievements of this work. Lastly, I am indebted to my parents and siblings for their unwavering support, which has been a constant source of inspiration and strength throughout this journey.

Annotation

Capillary waves play a vital role in destabilizing jets, films, and droplets. Understanding the growth rate of waves on electrified jets is essential for estimating break-up length and comprehending the transition from varicose to whipping instabilities in electrohydrodynamic jetting, specifically in the context of electrospinning. Moreover, the ripples formed by capillary waves in thin films and membranes significantly contribute to surface forces and interfacial tension, particularly near critical points. Despite their evident value and continuous research efforts since early 1900s, the widespread adoption of surface wave spectrometry has been impeded by technical complexities and the non-trivial interpretation of data.

The primary focus of this diploma thesis is to establish an experimental setup for observing surface phenomena of polymer solutions during DC electrospinning, a technique that utilizes electric fields to produce ultrafine fibers. The investigation involves analyzing the free surfaces using a technique based on the capillary wave profile. Specifically, two solvents (Water and Ethanol) and two commonly used polymer solutions Poly(vinyl alcohol) in water and Poly(vinyl butyral) in ethanol are examined to gain insights into the behavior of capillary waves within the context of electrospinning.

The observations made are then compared and studied in relation to classical theories in physics and electrospinning.

Keywords: *Capillary wave, Electrospinning, Laser, Polymer solution*

Anotace

Kapilární vlny hrají zásadní roli při destabilizaci proudů, filmů a kapek. Pochopení rychlosti růstu vln na elektrifikovaných tryskách je zásadní pro odhad délky rozpadu a rozpadu proudu a pochopení přechodu od varikózní k bičující nestabilitě v proudtech elektrohydrodynamických trysek, konkrétně v kontextu elektrostatického zvlákňování. Kromě toho vlnění tvořené kapilárními vlnami v tenkých vrstvách a membránách významně přispívá k povrchovým silám a mezifázovému napětí, zejména v blízkosti kritických bodů. Navzdory jejich zjevné hodnotě a nepřetržitému výzkumnému úsilí od počátku 20. století, bylo rozšířené přijetí spektrometrie povrchových vln ztíženo technickými složitostmi a netriviální interpretací dat.

Primárním cílem této diplomové práce je vytvořit experimentální uspořádání pro pozorování povrchových jevů polymerních roztoků při stejnosměrném elektrostatickém zvlákňování, což je technika využívající elektrická pole k výrobě ultrajemných vláken. Výzkum zahrnuje analýzu volných povrchů pomocí techniky založené na profilu kapilárních vln. Konkrétně jsou zkoumána dvě rozpouštědla (voda a etanol) a dva běžně používané polymerní roztoky (Poly(vinylalkohol) ve vodě a Poly(vinylbutyral) v etanolu), aby bylo možné získat vhled do chování kapilárních vln v kontextu elektrostatického zvlákňování. Provedená pozorování jsou poté porovnávána a studována ve vztahu ke klasickým teoriím ve fyzice a elektrostatickém zvlákňování.

Klíčová slova: kapilární vlna, elektrostatické zvlákňování, laser, polymerní roztok.

Content

| | |
|--|----|
| 1. Introduction | 14 |
| 2. Literature Review and Background Theory | 15 |
| 2.1. History of Electrospinning..... | 15 |
| 2.2. Principle of Electrospinning | 16 |
| 2.3. Electrospinning parameters..... | 17 |
| 2.4. Polymer Solution Parameters..... | 17 |
| 2.4.1. Concentration and Viscosity | 18 |
| 2.4.2. Surface tension and Capillary Pressure..... | 19 |
| 2.5. Process parameters..... | 21 |
| 2.5.1. Applied Voltage/Electrostatic potential | 21 |
| 2.5.2. Needle to collector distance and Orifice diameter | 21 |
| 2.6. External Forces | 23 |
| 2.6.1. Fluid pressure | 23 |
| 2.6.2. Electrostatic Pressure | 23 |
| 2.7. Fluid dynamics and Surface waves..... | 26 |
| 2.7.1. Gravity waves..... | 27 |
| 2.7.2. Capillary wave | 28 |
| 2.7.3. Damping of surface waves | 29 |
| 2.7.4. Jet instabilities..... | 30 |
| 2.7.5. Measuring techniques of Surface waves | 31 |
| 2.8. Laser Optics | 33 |
| 2.8.1. Working Principle of Laser..... | 33 |
| 2.8.2. Laser diffraction..... | 34 |
| 2.9. Polymers and Solutions used | 35 |
| 2.9.1. Poly(vinyl alcohol)(PVA) | 35 |
| 2.9.2. Poly(vinyl butyral)(PVB)..... | 36 |
| 2.10. Characteristics of the polymer solutions used..... | 37 |
| 2.10.1. Polymer Concentration..... | 37 |
| 2.10.2. Dynamic Viscosity | 37 |

| | |
|---|----|
| 3. Experimental part | 39 |
| 3.1. Materials and device setup..... | 40 |
| 3.1.1. Material details used in the setup..... | 41 |
| 3.2. Characteristic Experiment method..... | 42 |
| 3.3. Behavior of polymer solution and self organisation of jets in applied voltage... | 44 |
| 3.4. Data processing method | 45 |
| 3.4.1. Experiment with Water and Ethanol | 47 |
| 3.4.2. Experiment with PVA in Water | 51 |
| 3.4.3. Experiment with PVB in Ethanol..... | 54 |
| 4. Results | 57 |
| 4.1. Behavior of Water and Ethanol under Applied Voltage | 58 |
| 4.2. Mathematical parametric correlation in PVA | 59 |
| 4.3. Mathematical parametric correlation in PVB | 60 |
| 5. Conclusion..... | 61 |
| 6. Experiment limitations and suggestions | 62 |
| References | 63 |

List of abbreviations and symbols

| <i>abbreviation</i> | <i>Meaning</i> | <i>unite</i> |
|---------------------|------------------------------------|--------------------------|
| η | Coefficient of kinematic viscosity | [Ns/m ²] |
| γ | Surface Tension | [N/m] |
| σ | Surface charge density | [C/m ²] |
| ρ | Volume charge density | [C/m ³] |
| ϵ | Permittivity of air | [F/m] |
| ∇ | Gradient | |
| V | Electrostatic potential | [V] |
| E | Electric field intensity | [V/m] |
| g | Gravitational acceleration | [m/s ²] |
| ϕ | Velocity potential | [m ² /s] |
| ω | Angular frequency | [rad/s] |
| \bar{k} | Wave vector | |
| k | Wave number | [1/m] |
| λ | Wavelength | [m] |
| γ | Damping coefficient | [1/s] |
| φ | Applied voltage | [V] |
| cm | centimeter | [10 ⁻² meter] |
| mm | millimeter | [10 ⁻³ meter] |
| nm | nanometer | [10 ⁻⁹ meter] |
| kV | kilovolts | [10 ³ volts] |
| cP | centipoise | [10 ⁻² poise] |
| mW | Megawatts | [10 ⁶ watts] |

| | |
|----------------------------------|---|
| DC | Direct Current |
| MN | Minnesota |
| USA | United States of America |
| SAW | Surface Acoustic Waves |
| LASER | Light amplification by stimulated emission of radiation |
| PVA | Poly(vinylalcohol) |
| PVB | Poly(vinylbutyral) |
| H ₂ O | Water |
| C ₂ H ₅ OH | Ethanol |
| DSLR | Digital Single-Lens Reflex |
| UV | Ultraviolet |
| HV | High voltage |
| MATLAB | Matrix laboratory |

List of figures and graphs

| | |
|---|----|
| Figure 1: Schematic of DC capillary electrospinning device: Schematic of DC capillary electrospinning device: (1) syringe or metering pump outlet, (2) injection needle / capillary serving as spinning electrode, (3) stable part of polymer nozzle, (4) whipping zone of polymer nozzle, (5) collector, (6) ground, (7) high voltage source, the positive pole of which is connected to the capillary. Taken from [8]. | 16 |
| Figure 2. Polymer chain dimensions [11]. | 17 |
| Figure 3. Steric structure of chain [11]. | 18 |
| Figure 4. Viscous drag between two parallel plates [14] | 18 |
| Figure 5. (a) Graphical representation of the force action of molecules at the liquid-gas interface on the molecule in the center of the molecular sphere of action. Parts of Figures (a), (b), (c) and (d) show the increase in the resultant forces f with approaching the sphere of molecular action to the liquid-air interface. (b) The surface tension γ is the force acting perpendicular to the unit length of the imaginary section through the surface, which lies in a tangent plane to the surface at a given point. [8]. | 19 |
| Figure 6. Forces induced by surface tension acting on the surface of the cylinder. [8] | 20 |
| Figure 7. Schematic showing fluid pressure. | 23 |
| Figure 8. A charged, perfectly conductive drop has a normal n perpendicular to an elementary area, δS , of its surface. The total field strength, E , in the vicinity of the drop's surface is the sum of strengths $E1$ and $E2$. Particularly, $E1$ is the contribution to the total field strength, created by charges on a surface element, δS , and $E2$ is the contribution from all the resting charges on the sphere and from other charges in space. Point A is just outside the droplet, while point B is inside it. [8] | 24 |
| Figure 9. Wave breaking due to the effect of amplitude on propagation velocity. [21]. | 29 |
| Figure 10. Nonlinear effects in wave formation. [21] | 29 |
| Figure 11. Different types of jet instabilities during electrospinning. (a) Bending or whipping [22], (b) Rayleigh. Raleigh instability image [24], (c) Axisymmetric. [24]. | 30 |
| Figure 12. a) Surface wave taxonomy, b and c. Methods to generate and detect the properties of a wave. | 31 |
| Figure 13. Mechanism of LED and LASER illumination. (A) A microbeam of coherent laser light hits a specified target within a nematode, and (B) an incoherent beam of LED light illuminates the entire nematode as such [31]. | 33 |
| Figure 14. Polymer surface patterning by laser scanning [35]. | 34 |

| | |
|--|----|
| Figure 15. The sequence of reactions employed in the industrial manufacturing of poly(vinyl alcohol) (PVA) [36]..... | 35 |
| Figure 16. Structure of Poly(vinyl butyral) [38] | 36 |
| Figure 17. Viscosimeter used to measure dynamic viscosity..... | 37 |
| Figure 18. Experimental setup: A) Exciter; B) Laser; C) DSLR; D) UV Camera; E) Multimeter; F)Projection screen; G)Metallic container for polymer solution; H)Collector | 40 |
| Figure 19. A) DC electrospinning set up with incident laser beam; B) Surface of water without applied voltage on the projection wall | 41 |
| Figure 20. Path of light beam striking the convex mirror | 42 |
| Figure 21. A) Front view B) Back view of laser beam on convex mirror..... | 43 |
| Figure 22. Diffraction pattern of mirror on the screen | 43 |
| Figure 23. PVA solution with 10% concentration A) without applied voltage exhibiting a hemispherical/convex shape; B) and C) with voltage showing emerging jets, images captured under UV camera. | 44 |
| Figure 24. MATLAB screen..... | 45 |
| Figure 25. Measured illuminated height(d) in pixels. A and B without voltage, C and D at appearance of first corona discharge, with B and D showing the zoomed in images of A and B respectively | 46 |
| Figure 26. Diffraction pattern on surface of Water showing the surface wave propagations at A)5, B)10, C)15, D)20, E)25, F)30, and G)33.8(onset of jets) kV of applied voltage.... | 47 |
| Figure 27. Diffraction pattern on the surface of Ethanol showing the surface wave propagations at A)5, B)10, C)15, D)21, and E)25(onset of jets) kV of applied voltage..... | 48 |
| | |
| Graph 1. Dynamic Viscosities of PVA, PVB..... | 38 |
| Graph 2. Measurements with Water and Ethanol..... | 50 |
| Graph 3. Measurements with PVA..... | 53 |
| Graph 4. Measurements with PVB..... | 56 |
| Graph 5. Dependence of d[mm] on E^2 [kV ² /m] for PVA..... | 59 |
| Graph 6. Dependence of d[mm] on E^2 [kV ² /m] for PVB..... | 60 |

List of tables

| | |
|--|----|
| Table 1. Parameters that affect the elctrospinning process [10]..... | 17 |
| Table 2. Properties of used polymers | 37 |
| Table 3. Observed measurements converted in mm for each unit voltage value | 49 |
| Table 4. Surface phenomenon observed during the initial appearance of corona discharge in PVA | 51 |
| Table 5. Observed measurements converted in mm for each unit voltage value | 52 |
| Table 6. Correlation values between applied voltage[kV] and d[mm]..... | 53 |
| Table 7. Surface phenomenon observed during the initial appearance of corona discharge. | 54 |
| Table 8. Observed measurements converted in mm for each unit voltage value | 55 |
| Table 9. Correlation values between applied voltage[kV] and d[mm] for PVB | 56 |
| Table 10. Correlation values between Electrical intensity[kV ² /m ²] and d[mm] for PVA .. | 59 |
| Table 11. Correlation values between Electrical intensity[kV ² /m ²] and d[mm] for PVB... | 60 |

1. Introduction

Nanotechnology, which encompasses the comprehension and precise manipulation of matter at the nanoscale spanning from approximately 1 to 100 nanometers, unlocks exceptional phenomena and enables groundbreaking applications that were previously unattainable. [1] Electrospinning serves as a transformative nanotechnology platform, facilitating the creation of diverse and innovative structured materials with significant implications in numerous biomedical fields such as drug delivery, biosensing, tissue engineering, and regenerative medicine. [2]

Electrospinning is an effective nanofiber fabricating process that relies on the intricate interplay of surfaces, shapes, rheology, and electrical charge, which interact to generate electrified jets of polymer solutions and molten polymers. Charged ions, typically the carriers of charge, may exhibit varying velocities relative to changes in fluid shape. The Coulomb repulsion between these ions, within a fixed fluid quantity, favors the formation of jet-like structures, while fluid surface tension favors sphere-like shapes with lower surface area per unit mass. By increasing the surface's electrical potential to a sufficiently high level, electrical forces overcome and dominate the surface tension, resulting in the ejection of a charged fluid jet. [3]

Controlling the spatial orientation of nanostructures is essential for numerous applications, such as nanoscale device fabrication and tissue regeneration. [4] However, nanofibers are commonly gathered in the form of nonwoven mats, where the fibers exhibit a random orientation. [5] This disorder in the collected fibers arises from the unstable movement of the viscous jet during the electrospinning process. [6] Such instability of jet is caused by capillary waves. [3]

A capillary wave is a surface wave that propagates along the fluid interface between a liquid and air. Various techniques, including electromechanical and light scattering methods, have been employed to investigate and analyze capillary waves. The focus of this diploma thesis is to investigate the surface characteristics of polymer solutions during DC electrospinning using laser and verify the theoretical principles of physics and electrosopinning using observed phenomenon . The thesis is divided into two parts. The first part comprises a comprehensive literature review on electrospinning and its associated parameters. The

second part entails the design of the experimental setup and the evaluation of several polymer solutions under high voltage conditions.

2. Literature Review and Background Theory

2.1. History of Electrospinning

Electrospinning entails an electrohydrodynamic process wherein the application of an electrostatic field induces the movement of a fluid.

In 1600, William Gilbert made the initial observation of electrostatic attraction in liquids. In 1846, Christian Friedrich Schönbein successfully produced highly nitrated cellulose. The process of nano-fiber manufacture was described by Charles Vernon Boys in 1887 through a research paper. In 1900, John Francis Cooley filed the first patent for electrospinning. In 1914, John Zeleny published a seminal work on the behavior of fluid droplets at the terminus of metal capillaries, initiating the endeavor to mathematically model fluid behavior under electrostatic forces. From 1931 to 1944, Anton Formhals obtained a minimum of 22 patents related to electrospinning. In 1938, N.D. Rozenblum and I.V. Petryanov-Sokolov successfully generated electrospun fibers, which were further developed into filter materials. Between 1964 and 1969, Sir Geoffrey Ingram Taylor laid the foundation for the theoretical understanding of electrospinning by mathematically modeling the shape of the fluid droplet's (Taylor) cone under the influence of an electric field. In the early 1990s, various research groups, notably led by Reneker who popularized the term "electrospinning," demonstrated the production of electrospun nano-fibers. Since 1995, there has been an exponential increase in the number of scholarly publications on the topic of electrospinning. [7]

Electrospinning has garnered interest due to its potential for continuous production of nano-scale materials and its versatility with various processing materials. As of September 2007, notable commercialization in the industrial sector has been achieved by Donaldson Company Inc., Bloomington, MN, USA and Elmarco, Liberec, Czech Republic. However, the interdisciplinary nature of electrospinning, combining electrostatics, fluid dynamics, and physical chemistry, presents a significant hurdle for industry adoption.

2.2. Principle of Electrospinning

Process of Electrospinning involves creation of nanofibers through an electrically charged jet of polymer solution or melts. The simplest form of electrospinning consists of a pipette/syringe (Figure. 1) to hold the polymer solution, two electrodes (2, 5) and a DC voltage supply in the range of kV. Due to high voltage polymer nozzle is formed on the tip of the electrode (spinning), usually positively charged, having a very thin charged surface layer called “Debye Layer”. Further in the process, there is a stable part of polymer nozzle followed by the whipping zone resulting from electro-hydrodynamic instability. At the end, nanofibers are trapped on a negatively charged counter electrode called the collector. [8]

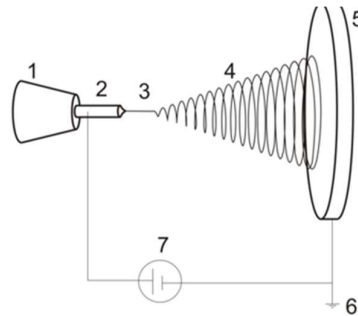


Figure 1: Schematic of DC capillary electrospinning device: Schematic of DC capillary electrospinning device: (1) syringe or metering pump outlet, (2) injection needle / capillary serving as spinning electrode, (3) stable part of polymer nozzle, (4) whipping zone of polymer nozzle, (5) collector, (6) ground, (7) high voltage source, the positive pole of which is connected to the capillary. Taken from [8].

Electrospinning results from imbalance of electrical and capillary forces. The disintegration of liquid bodies depends on the internal molecular structure. Molecules of low molecular weight disintegrate in clouds of electrically charged droplets which continue disintegration until a single elemental charge remains trapped [9]. Long slender liquid columns called polymer nozzles are formed through disintegration, which continue to elongate longitudinally due to the internal pressure of an enormous concentration of equally charged particles. This tendency to mechanically stretch the nozzle, together with its inertial weight and rheology, leads to a wild lateral movement of the nozzle, the so-called whipping. The nozzle lengthens enormously, causing it to rapidly reduce its projection, usually to a few hundred or tens of nanometers; narrowing the nozzle diameter results in increased curvature of its surface. The increase in curvature due to the decreasing radius causes an increase in capillary pressure inside the nozzle. The solvent is very efficiently expelled from the nozzle. [8]

In this work, surface behavior of polymer solutions is visualized under DC voltage supply.

2.3. Electrospinning parameters

There are numerous factors that govern the generation of smooth electrospun fibers for desired application. These can be classified as Process, Solution and Environmental parameters. Table.1 provides the overview of the parameters found in the literature. [10]

Table 1. Parameters that affect the electrospinning process [10]

| Solution Parameters | Process Parameters | Environmental parameters |
|---------------------|------------------------------|--------------------------|
| Concentration | Applied voltage | Temperature |
| Viscosity | Electric field strength | Humidity |
| Surface Tension | Electrostatic field shape | Local Atmosphere Flow |
| Conductivity | Needle to collector distance | Atmospheric Composition |
| Dielectric constant | Feed Rate | Pressure |
| Solvent volatility | Orifice diameter | |

For the purpose of this diploma thesis, few of the above process and solution parameters are explained in detail.

2.4. Polymer Solution Parameters

The term "polymer" derives from the Greek words "poly" meaning many and "mers" meaning particles. It denotes a molecule composed of multiple identical units known as mers, resulting in a macromolecular structure. In the realm of polymers, "many" typically refers to a minimum of several hundred mers. However, mechanical properties begin to manifest at around 30 mers, while polymers with an average length of 200-2,000 mers are commonly regarded as practical and functional. The molecular architecture of a polymer determines its shape and properties. A polymer chain can take on different forms depending on factors like temperature and solvent. In a theta state, the chain is like a randomly condensed coil that can expand with temperature or better solvent as shown in Figure 2. Polymer chains can have varying volumes under different conditions, represented by the end-to-end distance. This is important for measuring molecular weight using viscosity. [11]

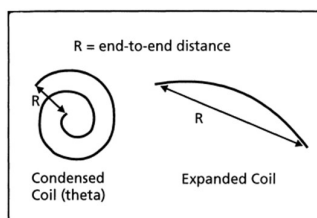


Figure 2. Polymer chain dimensions [11]

There are three main configurations as shown in Figure 3: linear, branched, and cross-linked chains. Linear chains have no branches, while branched chains have shorter side subchains that decrease crystallinity and viscosity. Longer branches can increase viscosity due to entanglements. Cross-linked chains have a lattice network structure, losing mobility and solubility. [11]

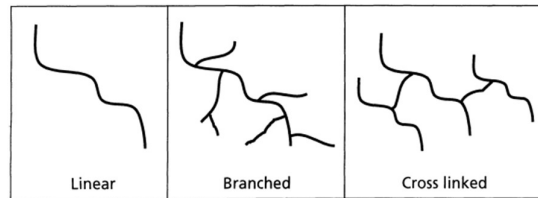


Figure 3. Steric structure of chain [11]

2.4.1. Concentration and Viscosity

Numerous significant studies have shed light on how solution concentration and viscosity impact the morphology of electrospun nanofibers.

The process of electrospinning relies on the phenomenon of a charged jet being stretched in one direction. The stretching of the charged jet is greatly influenced by the concentration of the polymeric solution. When the concentration of the solution is low, the electric field and surface tension cause the polymer chains to break into fragments before they reach the collector. This fragmentation leads to the formation of beads or beaded nanofibers. On the other hand, increasing the concentration of the polymeric solution increases its viscosity, promoting stronger entanglement among the polymer chains. These entanglements overcome surface tension, resulting in the production of uniform nanofibers without beads. However, if the concentration exceeds a critical value (the concentration at which beadless uniform nanofibers are formed), the solution becomes too viscous to flow smoothly through the needle tip. This can cause the polymer solution to dry at the tip of the metallic needle, blocking it and ultimately leading to defective or beaded nanofibers. [12] [13]

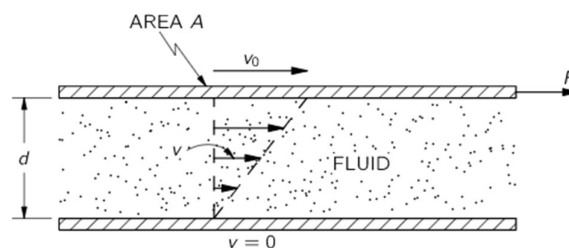


Figure 4. Viscous drag between two parallel plates [14]

Viscosity is a property that characterizes the shear forces within a flowing fluid. To quantify these shear forces, as depicted in Figure 4. Two solid plane surfaces with water are sandwiched. While keeping one surface stationary, the other surface is moved parallel to it

at a slow speed, denoted as v_0 . By measuring the force required to sustain the motion of the upper plate, it is observed that this force is proportional to the area of the plates and to v_0/d , where d represents the distance between the plates. Therefore, the shear stress (F/A) experienced is proportional to v_0/d . [14]

$$\frac{F}{A} = \eta \frac{v_0}{d}$$

Equation 1

The constant of proportionality η is called the coefficient of viscosity. SI Unit of Viscosity is $N\cdot s/m^2$

2.4.2. Surface tension and Capillary Pressure

For electrospinning to commence, the charged solution must overcome the effects of surface tension. Surface tension is a phenomena connected to the interface of various phases. The liquid-gas interface acts like an elastic thin layer because of the surface tension, trying to reconfigure the liquid's surface to have the least amount of area and, consequently, surface energy for a given volume. The surface tension is a result of the collective behaviour of fluid particles as a result of the tangential intermolecular forces. The cohesive pressure in the fluid is a result of normal components. [8]

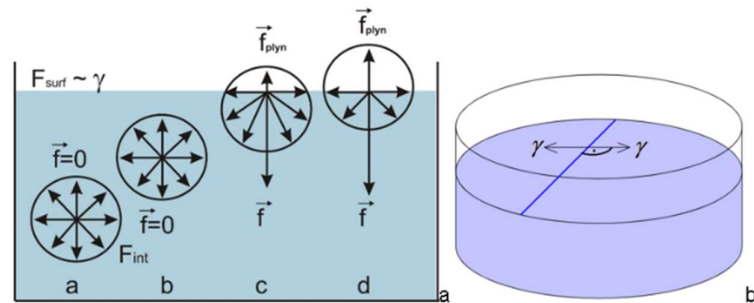


Figure 5. (a) Graphical representation of the force action of molecules at the liquid-gas interface on the molecule in the center of the molecular sphere of action. Parts of Figures (a), (b), (c) and (d) show the increase in the resultant forces \vec{f} with approaching the sphere of molecular action to the liquid-air interface. (b) The surface tension γ is the force acting perpendicular to the unit length of the imaginary section through the surface, which lies in a tangent plane to the surface at a given point. [8]

As shown in Figure 5, the depth of the liquid where the effect of asymmetric intermolecular activity is apparent is comparable to the diameter of the sphere of molecular action (c, d). It is on the order of a layer with a nanometer-thickness. Because applying a force along the path of displacement is required to move molecules from inside the liquid to the surface, or to do work to overcome the above-described resultant of intermolecular forces, the molecules in the surface layer have a higher potential energy than the molecules inside the liquid. Surface energy is the name given to this kind of free energy, W , which is determined by the relation [8]:

$$dW = \gamma dA$$

Equation 2

where dW is the change in surface energy of the system and dA is the increase in surface area of the liquid. The quantity γ denotes the surface tension, which also has the meaning of the surface energy density $\gamma = dW / dA$. The physical unit of surface tension is Nm^{-1} and the areal density of surface energy is Jm^{-2} . The surface tension γ can also be referred to as the force which acts perpendicular to the unit length of the imaginary section through the surface and which lies in a tangent plane to the surface at a given point. If a force dF acts on a line of length dl in the surface plane, then we express the surface tension as [8]:

$$\gamma = \frac{dF}{dl} \quad \text{Equation 3}$$

The SI unit of Surface tension is N/m.

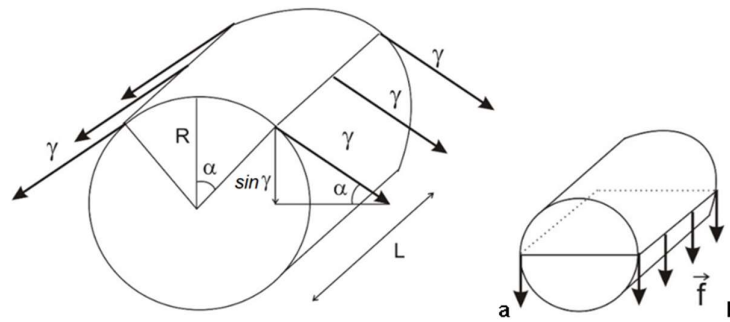


Figure 6. Forces induced by surface tension acting on the surface of the cylinder. [8]

Capillary pressure is produced due to the liquid's free surface's curvature. Consider a liquid with a curved surface S that resembles the shell of a cylinder (see Figure 6). If a portion of this mantle that has a length L is removed and is enclosed by arcs that are circular and measure a tiny angle α . Surface tension exerts a force along the two straight edges of the surface $S = 2LR$ that is perpendicular to the liquid's surface. The value of \vec{F} for its components acting perpendicular to surface S is $2\gamma L \sin(\alpha)$. $\sin(d\alpha) \approx d\alpha$ can be used to approximate a relationship for tiny angles d . The capillary pressure on the cylinder's surface can therefore be expressed as [8]:

$$p_c = \frac{2\gamma d\alpha L}{2R d\alpha L} = \frac{\gamma}{R} \quad \text{Equation 4}$$

The SI unit of Capillary Pressure is Pa.

2.5. Process parameters

2.5.1. Applied Voltage/Electrostatic potential

Exploring the impact of an external electrical force on the distance between the nozzle and collector in electrospinning offers a means to regulate the trajectory of the jet and the final deposition area. By investigating the transfer of charged particles, it becomes possible to manipulate the motion of the jet and the location of deposition, providing valuable insights for establishing electrospinning setups and designing auxiliary electrodes to control the deposition and alignment of nanofibers. To simulate the effect of the electric field on the path of the electrospinning jet, a steady-state charge distribution between the nozzle and collector can be employed. Within the electrospinning distance, the variation in electrostatic potential resulting from the charge distribution can be determined by solving the Poisson equation. This equation establishes a relationship between the electrostatic potential in a dielectric and the charge density present. [15]

The Poisson equation for the cartesian coordinate system is given by:

$$\Delta V = -\frac{\rho}{\epsilon} \quad \text{Equation 5}$$

where ϵ is the permittivity of air and ρ is the space charge density (in coulombs/m³). In general, values of V , ϵ , and ρ vary with position.

In classical physics, the electric force exerted on a unit charge in an electric field is referred to as electric field intensity or field intensity, while the electrical state involving the flow of charge between two charged bodies is known as electric potential. Equation 6 establishes the relationship between electric potential (V) and electric field intensity (E), stating that E can be obtained by taking the gradient of V at a specific point, with a change of sign

$$E = -\nabla V \quad \text{Equation 6}$$

In general, the electric field strength needed to initiate electrospinning typically falls within the range of 0.5 to 1.5 kV/cm. However, if the localized electric field surpasses the dielectric strength of the surrounding atmosphere, it can lead to the generation of a corona discharge.

2.5.2. Needle to collector distance and Orifice diameter

The distance between the tip and collector in electrospinning has a notable impact on the trajectory of the jet and the duration it takes for the fibers to settle on the collector. When the voltage is held constant, the strength of the electric field becomes inversely proportional to the distance. In a typical electrospinning configuration, this distance typically falls within the range of 10 to 15 cm, allowing sufficient time for the solvent to evaporate and resulting

in the deposition of dry fiber strands. Additionally, when the voltage remains constant while the distance is altered, the behavior of the electrospinning jet and the resulting fiber profile resemble those observed when the voltage is adjusted while maintaining the tip-to-collector distance. Increasing the separation between the tip and collector may lead to a reduction in fiber diameter as the stretching distance becomes greater [16]. However, beyond a certain distance, the fiber diameter may instead increase due to a significant weakening of the electric field strength [17].

Furthermore, the evaluation of the orifice diameter for the spinning head's design has been explored by various authors. Their findings indicated that the utilization of larger orifices led to the production of thicker fibers. Conversely, excessively large orifices posed challenges in maintaining a stable Taylor cone, while extremely small orifices became impractical due to the drying out of the Taylor cone or the excessively high viscosity of the polymer hindering its flow [18].

2.6. External Forces

The electrospinning process and the resulting nanofiber morphology are primarily influenced by the properties of the polymer solution. Subsequently, the external forces employed to shape the polymer solution into a jet. In this section Fluid and Electrostatic pressures are explained.

2.6.1. Fluid pressure

In electrospinning, a commonly employed method involves utilizing a syringe pump to ensure a controlled volume flow rate under constant pressure.

The hydrostatic pressure, which arises from the weight of the fluid as depicted in Figure 7, above a specific point in the pipette tube, can be expressed as follows:

$$P = \rho gh \qquad \text{Equation 7}$$

ρ is the density of the fluid, g is the gravitational acceleration and h is the depth below the surface.

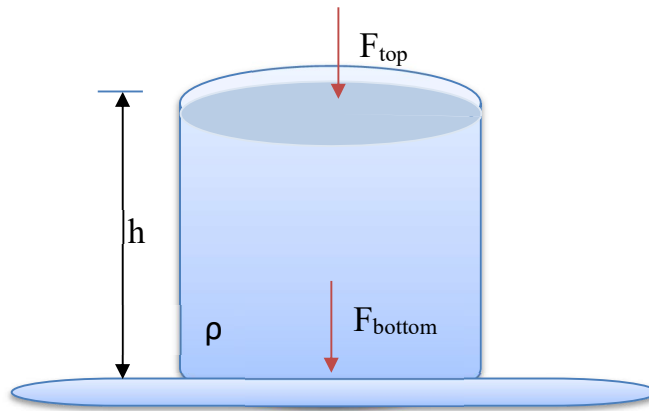


Figure 7. Schematic showing fluid pressure

2.6.2. Electrostatic Pressure

Electrospinning involves the application of charges to the solution, whereby the primary forces responsible for thinning the polymer solution jet are the repulsion force and the electrical force. The repulsion forces induce instability and whipping motions, and their magnitude relies on the properties of the polymer and solvent employed. On the other hand, the electrical force is responsible for elongating the jet and propelling it towards the grounded collector, and its strength is determined by the applied electric field and the material characteristics. Electrostatic pressure acts on the droplet surface by external electric field. Derivation of the electric pressure is provided below.

Considering two extremely close points A and B near the surface of an electrically charged conductive liquid in the form of a drop, see Figure 7 (a). The first is outside the liquid just above its surface. The second point is located inside the liquid, also near its surface. Let \vec{E}_1 and \vec{E}_2 be contributions to the total field strength \vec{E}_1 at points A and B. The electric field intensity \vec{E}_1 is generated by a charge located on the surface element of the droplet ds , while the intensity \vec{E}_2 is generated by all charges not located on this planar element, i.e., all other charges "in space". [8]

Figure 8. provides a detailed description of electric field strength acting on the charged liquid surface.

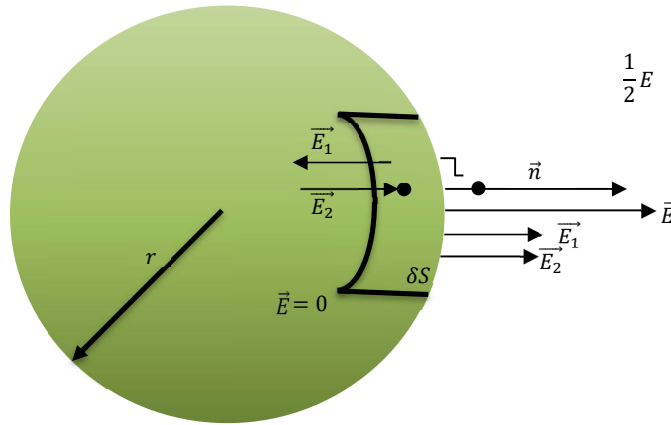


Figure 8. A charged, perfectly conductive drop has a normal \vec{n} perpendicular to an elementary area, δS , of its surface. The total field strength, \vec{E} , in the vicinity of the drop's surface is the sum of strengths \vec{E}_1 and \vec{E}_2 . Particularly, E_1 is the contribution to the total field strength, created by charges on a surface element, δS , and E_2 is the contribution from all the resting charges on the sphere and from other charges in space. Point A is just outside the droplet, while point B is inside it. [8]

The orientation of the total field strength vector must be perpendicular to the conductor surface under equilibrium conditions, i.e., under electrostatic conditions. In addition, inside the conductive liquid, the electric field strength is zero $\vec{E}(B) = 0$. The perpendicular to the liquid surface is also assumed for the vector of the contribution of the electrostatic intensity \vec{E}_1 because the charge distribution on the infinitesimal element of the surface area of the drop ds is homogeneous. Since inside the conductive liquid the total electric field intensity $\vec{E}(B)$ is zero, the vectors $\vec{E}_1(B)$ and $\vec{E}_2(B)$ must be collinear for their vector sum inside the liquid to give zero, i.e., $\vec{E}_2(B) - \vec{E}_1(B) = 0$. From this it is obvious that the vector \vec{E}_2 is perpendicular to the surface of the liquid. Due to the collinearity of all three intensity vectors, \vec{E}_1 , \vec{E}_2 and \vec{E} further analysis can be performed with absolute values of field intensities

instead of their vector nature. We can construct two simple algebraic equations for the field intensities at points A and B. At point B inside the conductive fluid, the following relation holds:

$$E(B) = E_2(B) - E_1(B) = 0 \quad \text{Equation 8}$$

and at point A outside the liquid applies:

$$E(A) = E_1(A) - E_2(A) = 0 \quad \text{Equation 9}$$

Due to the small distance between points A and B , absolute values can be obtained E_1 considered the same at these points. The same goes for values E_2 . Since the intensity of E_1 is generated by the surface charge, the orientation of the vector E_1 outside and inside the drop is opposite, as expressed by the change of the sign of E_1 in equations above. The intensity E_2 generated by the charge in the rest of the liquid body and beyond does not change the orientation as it passes through its surface. A direct consequence of equations above is:

$$E_1 = E_2 = \frac{1}{2}E \quad \text{Equation 10}$$

Application of the Gaussian electrostatic theorem for the Gaussian surface of the cuboid shape surrounding the surface of the surface element ds , provides the following relationship:

$$E ds = \frac{\sigma ds}{\epsilon} \quad \text{Equation 11}$$

We emphasize that in the Gaussian theorem electrostatic we always consider the flow of the total field intensity \vec{E} . The electric pressure p_e is the force acting on the unit surface area of the spherical droplet, and is therefore determined by the usual relation, $p_e = dF/ds$. The force dF is given by the product of the magnitude of the charge E_2 , i.e., $\sigma ds E_2$ on the surface element ds and the intensity of the electrostatic.

$$p_e = \frac{\sigma ds E_2}{ds} \quad \text{Equation 12}$$

By substituting for σ in above equations we express the electric pressure p_e on the surface of conductive bodies by the relation [8].

$$p_e = \frac{1}{2} \epsilon E^2 \quad \text{Equation 13}$$

The SI unit of Electrostatic Pressure is Pa.

2.7. Fluid dynamics and Surface waves

Study by Prof. Lukas et al. [19] explores electrospinning from conductive liquids' free surfaces and validates a formulated hypothesis that explains the self-organization of jets on one-dimensional liquid surfaces. This phenomenon is attributed to the electrohydrodynamic instability of surface waves. By conducting a thorough analysis of a dispersion law, the hypothesis proposes that when the applied electric field intensity exceeds a critical value, the system undergoes self-organization on a mesoscopic scale through the mechanism of the "fastest forming instability." This mechanism plays a crucial role in selecting a specific wave with a characteristic wavelength, whose amplitude grows infinitely faster than the others. According to the hypothesis, the onset of electrospinning from a free liquid surface occurs with jets originating from the wave crests.

A simplified approach to understanding the mechanics of stable electrospinning jets is based on electrohydrodynamic theory that explicitly incorporates the extensional rheology of polymeric fluids. Surface waves refer to mechanical waves that travel along the boundary between different media. The behavior of these waves is influenced by either gravity or surface tension, depending on their period. In this section, a detailed explanation and derivation of capillary waves is provided, which are particularly significant for the purpose of this study.

Fluid dynamics concerns itself with the study of motion of fluids (liquids and gases). The behavior of an ideal fluid, one without viscosity, can be described by Euler's equation, initially formulated by L. Euler in 1755.

$$\frac{dv}{dt} + (v \cdot \text{grad})v = -\frac{1}{\rho} \text{grad } p \quad \text{Equation 14}$$

Here, dv/dt represents the rate of change of fluid velocity at a fixed point in space, ρ denotes the density of the fluid, and $\text{grad } p$ represents the force acting on a unit volume of the fluid with p being pressure.

When the fluid is subjected to a gravitational field, an additional force comes into play, altering the equation to the following form

$$\frac{dv}{dt} + (v \cdot \text{grad})v = -\frac{\text{grad } p}{\rho} + g \quad \text{Equation 15}$$

In the above derived equations of motion, no consideration is given to the processes of energy dissipation that may occur in a moving fluid due to internal friction (viscosity) or heat exchange between different parts of the fluid. These equations are valid only for the motion of fluids in which thermal conductivity and viscosity play a negligible role. Such fluids are referred to as ideal. [20]

2.7.1. Gravity waves

When a liquid is in equilibrium within a gravitational field, its free surface is flat like a plane. However, if an external disturbance affects the surface at a certain point, motion will be initiated within the liquid. This motion propagates across the entire surface, giving rise to a phenomenon known as gravity waves. These waves are a result of the gravitational forces acting on the liquid. While gravity waves primarily manifest on the surface of the liquid, they also influence the interior, albeit with diminishing impact as the depth increases. [20]

When a plane free liquid surface is in equilibrium within a gravitational field, any departure from equilibrium results in oscillatory motion called gravity or capillary waves. These waves propagate along the liquid surface, maintaining a constant wavelength between points with identical phases. If the oscillation amplitude is small compared to the wavelength, the motion can be considered potential. In the presence of the gravitational field $\rho g z$, the motion can be described by the equation.

$$p = -\rho g z - \rho \frac{d\phi}{dt} \quad \text{Equation 16}$$

where p is the pressure, ρ the density, g the acceleration due to gravity, ϕ the velocity potential, the z axis is perpendicular to the plane liquid surface (x, y).

The solution of this equation has the form of a plane harmonic wave

$$\phi = A e^{-\bar{k}z} \cos(\bar{k}x - \omega t) \quad \text{Equation 17}$$

where ω is the angular frequency, \bar{k} the wave vector ($\bar{k} = \bar{n}k$, where \bar{n} is the unit vector, k the wave number, $\lambda = 2\pi/k$ the wavelength).

When the pressures on a liquid surface and in the surrounding environment are equal, a boundary condition is established. This condition relates the frequency and wave vector through a dispersion equation, $\omega^2 = kg$. Liquid particles exhibit circular motion around an equilibrium point, with the radius of the circles exponentially decreasing as one moves

deeper into the liquid. The rate at which the amplitude distribution profile in a wave displaces is determined by the group velocity, $U = \partial\omega/\partial k$, where ω is the frequency and k is the wave vector. When the ω - k relationship is linear, the group velocity coincides with the phase velocity, $U = \omega/k$. For short gravity waves in a liquid, the group velocity depends on the wavelength and can be expressed as:

$$1/2 \sqrt{g/k} = 1/2 \sqrt{g\lambda/2\pi} \quad \text{Equation 18}$$

where g represents the acceleration due to gravity.

In the case of long gravity waves, where the wave length is much larger than the liquid depth h_0 , transverse waves may appear in a viscous liquid. In these waves, liquid particles move perpendicular to the wave propagation, rather than in circular paths. These waves arise when a body submerged in a viscous liquid undergoes oscillations. [20] [21]

2.7.2. Capillary wave

Capillary waves play a significant role in triggering various destabilization mechanisms in jets, films, and droplets.

Fluid surfaces tend to assume an equilibrium shape, both under the action of the force of gravity and under that of surface tension forces.

Taking into account surface tension forces γ , the dispersion equation takes the form:

$$\omega = \sqrt{gk + \gamma k^3/\rho} \quad \text{Equation 19}$$

where ρ is the density of the liquid. Surface tension forces have a significant impact on very short waves, such as ripples.

When dealing with waves of short wavelengths, the influence of gravity can be disregarded, resulting in what are known as capillary waves or ripples. [20]

$$\omega = \sqrt{\gamma k^3/\rho} \quad \text{Equation 20}$$

When a finite-amplitude disturbance occurs on the surface of a liquid, it propagates as a simple or Riemann wave. The velocity of displacement for points with equal phases on the wave relies on the amplitude and sign of the disturbance. As a result, the wave profile undergoes continuous deformation. Specifically, points with greater amplitudes propagate at a faster rate, causing the wave crest to catch up with its foot. The steepness of the front slope

intensifies, and when a critical height is reached, the wave collapses, forming capillary ripples or white caps as shown in Figure. 9. [21]

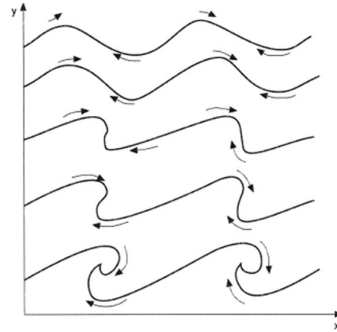


Figure 9. Wave breaking due to the effect of amplitude on propagation velocity. [21]

In regions characterized by an exceptionally steep profile, both dispersion and dissipation have a significant impact. Dissipation plays a role in the gradual smoothing of the saw-tooth pattern exhibited by the wave. Within this context, stationary waves can emerge as a series of short pulses. These waves arise due to the interplay between nonlinear effects, the "overturning" of the wave profile, and the influence of dispersion, which contributes to the broadening of the profile (refer to Figure 10). [21]

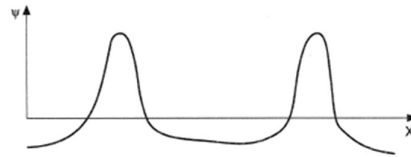


Figure 10. Nonlinear effects in wave formation. [21]

2.7.3. Damping of surface waves

Damping of surface waves refers to the reduction of the amplitude of these waves over time, preventing its oscillation. In physical systems, damping is produced by processes that dissipate the energy stored in the oscillation. The damping of waves is conveniently characterized by the damping coefficient γ . In the clean-surface scenario, the damping rate is typically $2\eta k^2$, where ν represents the kinematic viscosity and k is the wavenumber (equal to 2π divided by the wavelength).

However, when viscoelastic films are present, the damping rate increases due to changes in the boundary condition for the tangential stress component given by equation 21.

$$\gamma = 2\eta \frac{\omega^4}{g^2} \tag{Equation 21}$$

where, γ is the damping coefficient, η is then kinematic viscosity, ω is the angular frequency and g is the gravitational acceleration. [20]

2.7.4. Jet instabilities

During the process of Electrospinning, the emerging jet gradually becomes thinner as it moves towards the collector. However, this narrowing of the jet can result in a dominant radial charge repulsion caused by variations in the charge density. As a consequence, the jet undergoes turbulent motion around its axis, referred to as the "bending" or "whipping" instability. This instability plays a significant role in elongating the fibers and reducing their diameter within this region. Additionally, the radial charge repulsion can cause the primary jet to split into thinner jets, known as "splaying," leading to the formation of finer fibers. [22]

In the electrospinning process, three types of axisymmetric instabilities have been observed. Firstly, there is the classical "Rayleigh" instability, which is governed by the liquid's surface tension and can occur even without an electric field. This instability causes the liquid stream to break up into small droplets, potentially contributing to the formation of beads [23]. Rayleigh demonstrated that a liquid jet with an initial radius (r_0) disintegrates due to perturbations caused by waves of different wavelengths (λ) on the surface of the liquid column, where λ is always greater than $2\pi r$. The disintegration of the cylindrical liquid film proceeds rapidly, following the mechanism of the fastest-forming instability. The self-organization of jets in electrospinning is believed to be based on this fastest-forming instability.

Secondly, there is the "electric field induced" instability, which is influenced by the charge density of the solution. This instability becomes more pronounced as the charge density decreases, leading to variations in the surface charge density of the jet. Consequently, periodic "beads" can form along the fiber axis, resulting in defects and interruptions in the fiber structure [24].

The contribution of these three instabilities depends on the properties of the fluid and the operating parameters, as demonstrated by Shin et al in Figure. 11.

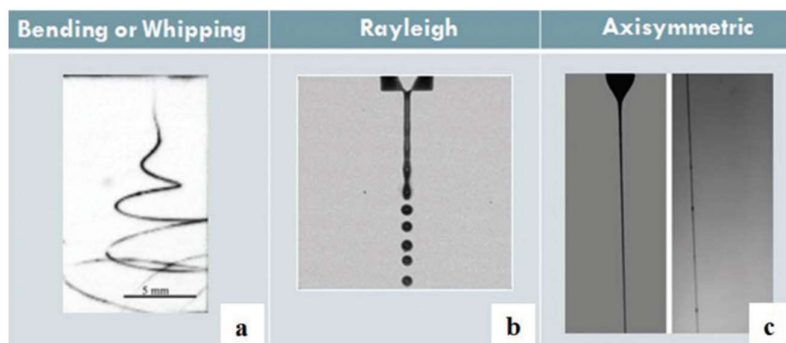


Figure 11. Different types of jet instabilities during electrospinning. (a) Bending or whipping [22], (b) Rayleigh. Raleigh instability image [24], (c) Axisymmetric. [24]

2.7.5. Measuring techniques of Surface waves

There is a multitude of waves that can be found at the boundary between two fluids. Numerous methods have been employed to investigate surface/capillary waves. Initially, the electromechanical technique [25] was used to measure the wavelength and damping coefficient of capillary waves when the amplitude-to-wavelength ratio was low. However, nowadays, light scattering techniques are the most commonly used methods for measuring the wavelengths and damping coefficients of capillary waves. Experimental approaches for studying liquid SAWs (Surface acoustic waves) have primarily utilized methods based on light reflection or scattering. For instance, in 1979, Weisbuch and Garbay treated liquid SAWs as a diffraction grating and developed an optical method to detect liquid surface tension [26].

A rigorous review by Ismail et al. [27], has been done on the current state of art of the methods to study capillary waves. Figure 12 provides Taxonomy of Surface waves.

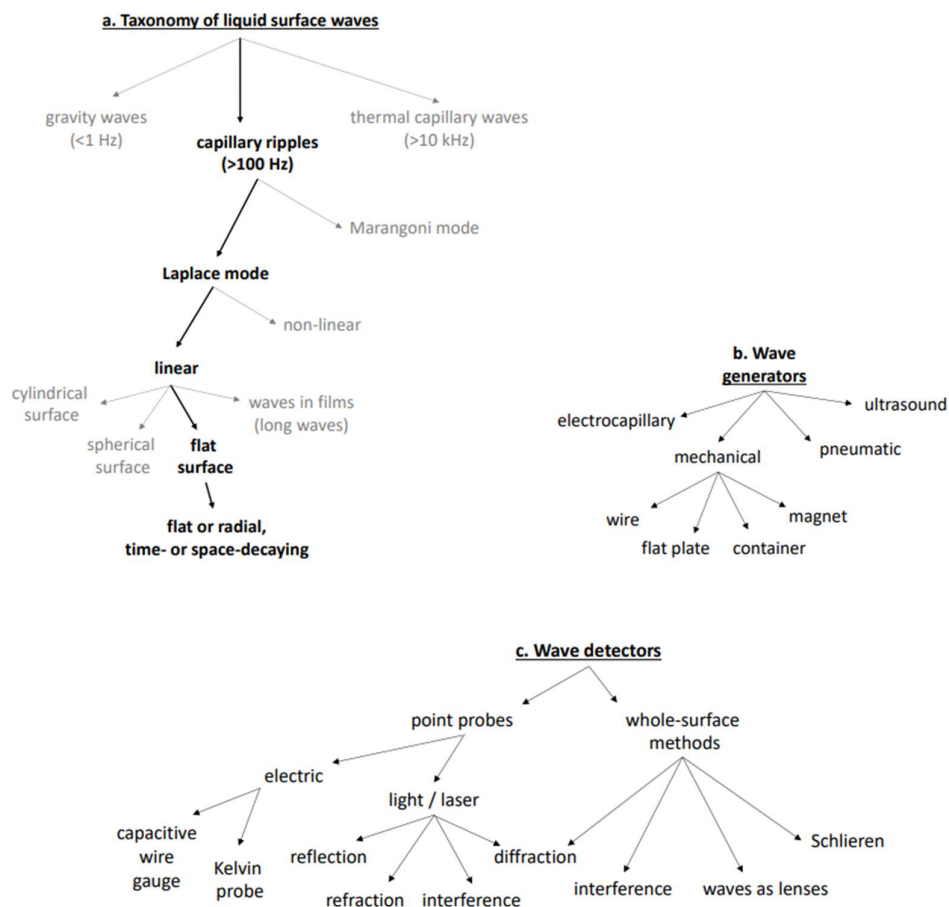


Figure 12. a) Surface wave taxonomy, b and c. Methods to generate and detect the properties of a wave.

Two different light scattering methods widely in use are explained below:

i. Dynamic light scattering technique

This method involves studying the time autocorrelation function of light that is scattered by thermally excited surface waves. These measurements do not introduce mechanical disturbances, and the surface waves caused by thermal fluctuations naturally decay over time [28]. The optical setup determines the selected wave number (k) of the capillary waves, and the observed photon correlation spectrum provides the corresponding complex frequency. The imaginary part of the spectrum represents the damping of the capillary waves.

ii. Capillary wave profile technique

In this approach, surface waves are generated at a specific real frequency ω . The resulting capillary waves are detected by measuring the oscillation of a reflected laser beam, which is deflected by the time-dependent surface profile [29]. By measuring the surface wave profile as a function of distance from the source of excitation, the complex wave number ($k = \alpha + i\beta$) of a capillary wave can be determined. The decay in wave amplitude as the waves propagate along the surface is represented by the damping factor β .

This thesis work designs the experiment based on capillary wave profile technique to observe diffraction and interference patterns on the free surface of polymer solutions used to produce nanofibers in DC electrospinning using laser light scattering.

2.8. Laser Optics

The fundamental principles of lasers were initially formulated by American scientist Charles Hard Townes, as well as Soviet scientists Alexander Mikhailovich Prokhorov and Nikolai Gennediyevich Basov, who collectively received the prestigious Nobel Prize in 1964. However, it was TH Maiman of the Hughes Research Laboratory in California who conducted the first experimental demonstration of a laser by directing light through a ruby crystal in 1960 [30].

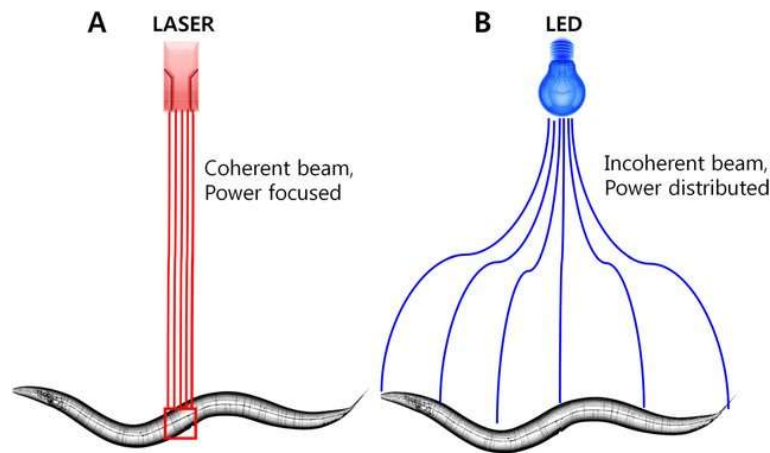


Figure 13. Mechanism of LED and LASER illumination. (A) A microbeam of coherent laser light hits a specified target within a nematode, and (B) an incoherent beam of LED light illuminates the entire nematode as such [31].

The word “laser,” is an acronym for light amplification by stimulated emission of radiation. Unlike conventional light sources such as tungsten lamps or mercury lamps, lasers possess remarkable properties. One notable characteristic is their ability to emit light waves that can travel long distances with minimal divergence as shown in Figure.13. In contrast, ordinary light sources emit a chaotic combination of individual waves that randomly interfere with each other, resulting in limited travel distances [32].

2.8.1. Working Principle of Laser

According to quantum theory, every atom has discrete energy levels or states. Typically, atoms exist in the lowest energy state, known as the ground state. However, when atoms are exposed to intense light from a source like a flash lamp or a mercury arc, they can be excited to higher energy levels. This phenomenon is called absorption. After a brief period

(approximately 10^{-8} seconds) in the excited state, the atom returns to its ground state, releasing a photon in the process. This emission is known as spontaneous emission.

In a conventional light source, both absorption and spontaneous emission occur. If an atom, still in its excited state, is struck by an external photon with precisely the energy required for spontaneous emission, the external photon combines with the one emitted by the excited atom. Additionally, both photons are released from the same excited state and are in phase with each other. This process is called stimulated emission and plays a fundamental role in laser operation. Through stimulated emission, the atom is encouraged or induced to emit its photon earlier than it would have under spontaneous emission alone. The laser can be compared to a spring that is wound up and ready to be released. The key to triggering it is a photon with the exact wavelength of the desired emitted light [33].

In this work, a green laser with wavelength of 532nm, output power of 100mW and working voltage of DC3.7V was used to light the surface of the polymer solutions.

2.8.2. Laser diffraction

Francesco Grimaldi (1618-1663) was the first to discover and document the phenomenon known as diffraction of light. In his experiments, he observed that when light passed through a small aperture, it did not simply travel in a straight line as particles would, but instead spread out in the form of a cone [34]. This observation provided compelling evidence for the wave nature of light.

Diffraction of light around an object's many surfaces causes interference effects, which result in a fuzzier shadow of the object. When light encounters surfaces, various phenomena can occur, including refraction, reflection, absorption, or diffraction. Laser diffraction is based on the interplay between light and surfaces. Figure 14 illustrates Laser light (633 nm) passing through lattices on PMMA (1500K) doped with 3% porphyrine creates a diffraction pattern.

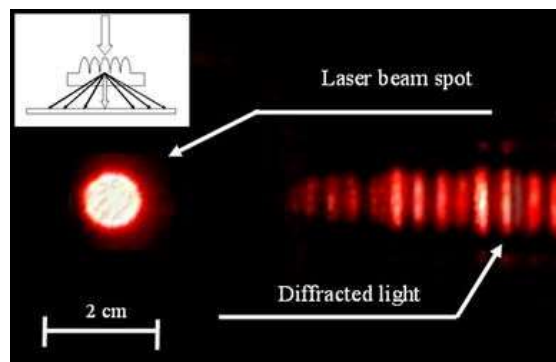


Figure 14. Polymer surface patterning by laser scanning [35]

2.9. Polymers and Solutions used

In this work, two solvents and three commonly used polymer solutions' free surfaces were analyzed which are Water, Ethanol and Poly(vinyl alcohol) in water), Poly(vinyl butyral) in ethanol, polyvinylpyrrolidone in ethanol and water respectively PVA and PVB solutions with concentrations of 8%, 10%, and 12% were meticulously prepared through dissolution in water and ethanol, respectively. The solutions were subjected to thorough mixing using a hot plate equipped with a magnetic stirrer for a duration of 24 hours. Additionally, two PVP solutions with a concentration of 10% were prepared by dissolving the polymer in water and ethanol, following the same mixing procedure. Comprehensive descriptions of each polymer can be found in the subsequent sections.

2.9.1. Poly(vinyl alcohol)(PVA)

Poly(vinyl alcohol) used in commercial applications is produced from poly(vinyl acetate) as shown in Figure 15. The molecular weight of commercial poly(vinyl alcohol) varies depending on the desired viscosity grade.

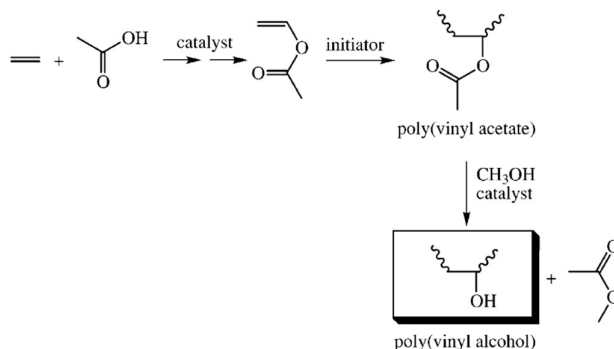


Figure 15. The sequence of reactions employed in the industrial manufacturing of poly(vinyl alcohol) (PVA) [36].

Here are the typical molecular weight ranges for different viscosity grades and their corresponding viscosities in a 4% aqueous solution:

- Low viscosity grade: Molecular weight (Mn) around 25,000, resulting in a viscosity range of 5-7 cP.
- Intermediate viscosity grade: Molecular weight (Mn) around 40,000, resulting in a viscosity range of 13-16 cP.
- Medium viscosity grade: Molecular weight (Mn) around 60,000, resulting in a viscosity range of 28-32 cP.
- High viscosity grade: Molecular weight (Mn) around 100,000, resulting in a viscosity range of 55-65 cP.

These viscosity values refer to a 4% aqueous solution of poly(vinyl alcohol) [37].

Poly(vinyl alcohol) (PVA) stands out among vinyl polymers as it exhibits water solubility and is capable of undergoing complete biodegradation when exposed to appropriately acclimated microorganisms.

For the purpose of this work, below product of PVA was utilized.

Name: Sloviol R 16%

Supplier: FICHEMA sro

2.9.2. Poly(vinyl butyral)(PVB)

Poly(vinyl butyral) (PVB) belongs to the poly(vinyl acetal) resin family. It is produced by condensing poly(vinyl alcohol) (PVA) with butyraldehyde in the presence of a potent acid catalyst. During the reaction, PVA and the aldehyde combine to form primarily six-membered rings, predominantly connecting adjacent hydroxyl groups within the same polymer chain [38].

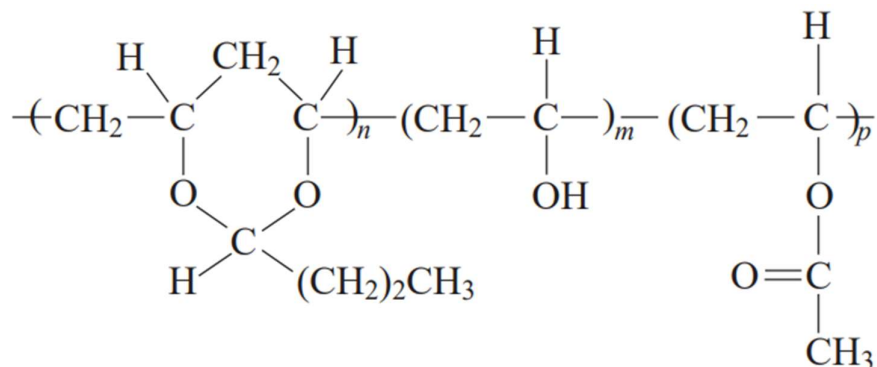


Figure 16. Structure of Poly(vinyl butyral) [38]

Poly(vinyl butyral) (PVB) is a polymer that possesses desirable characteristics, making it biocompatible, non-toxic, and odorless. It demonstrates excellent solubility in alcohol and inorganic substances, resulting in versatile applications. PVB also offers enhanced flexibility and exhibits strong adhesion to a wide range of substrates.

For the purpose of this work, below product of PVB was utilized.

Name: Butyral resin

Grade: Mowital B 60H

Brand: Mowital™

Producer: Kuraray

2.10. Characteristics of the polymer solutions used

2.10.1. Polymer Concentration

Eight polymer solutions were prepared. PVA and PVB solutions were prepared in water and ethanol respectively, at three concentration levels- 8%, 10%, and 12%.

2.10.2. Dynamic Viscosity

All the polymer solutions were investigated for dynamic viscosity at temperature of 22° C in the Thermo Scientific HAAKE RotoVisco 1 (shown in Figure 17).

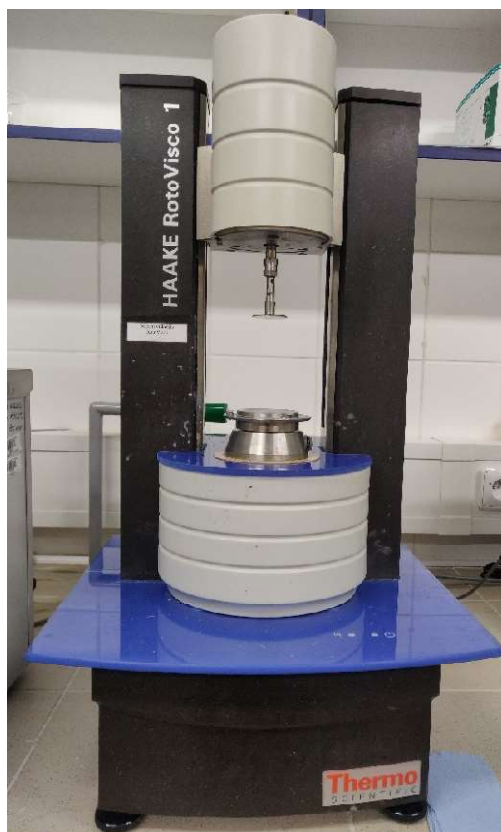


Figure 17. Viscosimeter used to measure dynamic viscosity

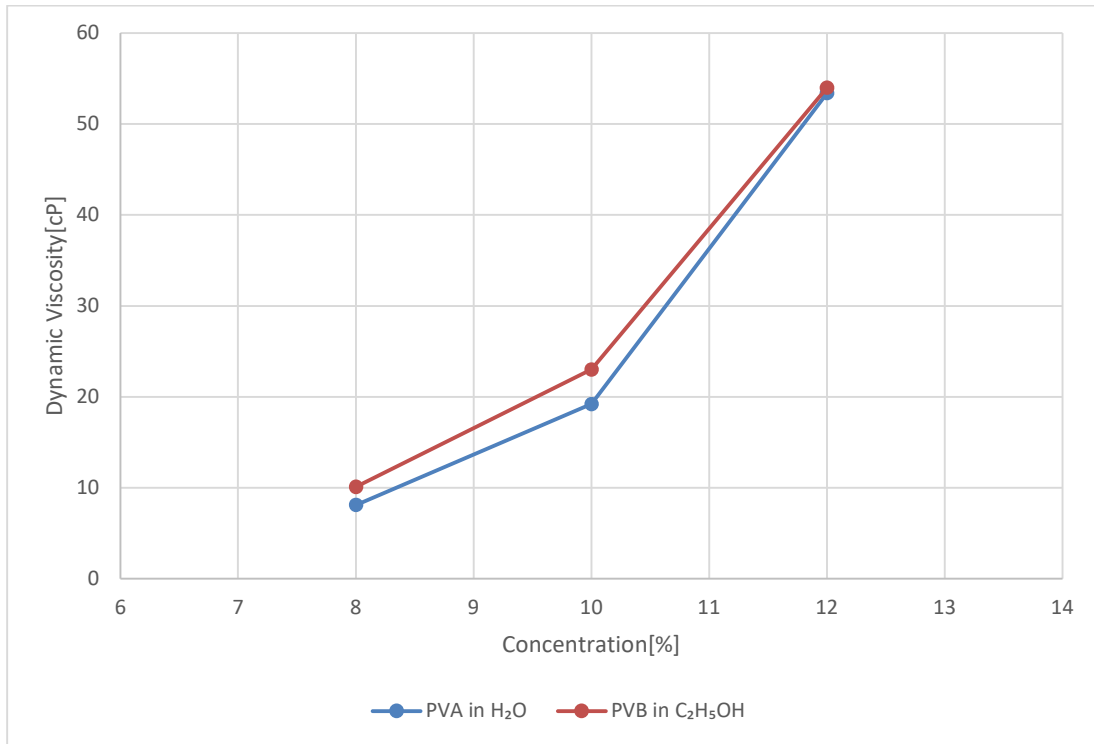
A total five trials were done for each of the solutions and the mean dynamic viscosity was evaluated.

Table 2. Properties of used polymers

| | Polymer Solution | Concentration[%] | Mean Dynamic Viscosity[cP] |
|----|-------------------------|------------------|----------------------------|
| 1. | PVA in H ₂ O | 8 | 8.1 |
| 2. | | 10 | 19.2 |
| 3. | | 12 | 53.4 |

| | | | |
|----|---|----|------|
| 4. | | 8 | 10.1 |
| 5. | PVB in C ₂ H ₅ OH | 10 | 23 |
| 6. | | 12 | 54 |

Graph 1. illustrates a positive correlation between concentration and dynamic viscosities of PVA and PVB.



Graph 1. Dynamic Viscosities of PVA, PVB

3. Experimental part

The primary objective of this thesis is to develop a device setup capable of facilitating the observation of surface phenomena, with a specific focus on the diffraction patterns exhibited by capillary waves in polymer solutions when subjected to high voltage.

The experimental design involves the development of a DC electrospinning setup that allows for the manipulation of various adjustable parameters, including the laser pointer and working distance. To ensure optimal visualization of the polymer solution, a metallic container with an enlarged orifice diameter is specifically designed to facilitate the passage of the laser beam. The surface dynamics resulting from the application of varying voltages are recorded using a digital single-lens reflex camera(DSLR). To visually represent the applied voltage in each recorded frame, a multimeter is positioned within the camera's field of view. Additionally, a UV camera is utilized to identify the critical voltage at which the first corona discharge occurs, subsequently initiating the formation of nanofibers.

The observed surface phenomenon is hypothesized to be the amplitude of interference surface waves. The amplitude data corresponding to each unitary applied voltage is recorded and subsequently analyzed using MATLAB. The analysis aims to establish correlations between the experimental data and theoretical entities, thereby examining the underlying relationships between the observed surface wave amplitudes and the expected theoretical behavior.

3.1. Materials and device setup

Figure 18 presents a schematic diagram of the experimental setup employed in this study. Prepared solutions were contained within a metallic container with an orifice diameter of 3,685 cm and a depth of 1 cm positioned on electrode. Working distance has been kept as 10 cm. External excitation in the polymer solution was achieved by applying voltage through a high voltage source. The electric potential between the electrodes was manually increased by adjusting the knob on the high voltage source. To visualize the surface propagations, a green laser was directed onto the surface of the polymer solution, and the resulting reflected light beams were projected onto a screen. The experiment took place in a basement setting to mitigate damping effects, with the wall serving as the projection screen. Visual dynamics were recorded in the form of videos using a DSLR camera, capturing 60 frames per second. In order to determine the critical electrical intensity associated with each polymer solution, corona discharges and taylor cones were visualized using a UV camera.

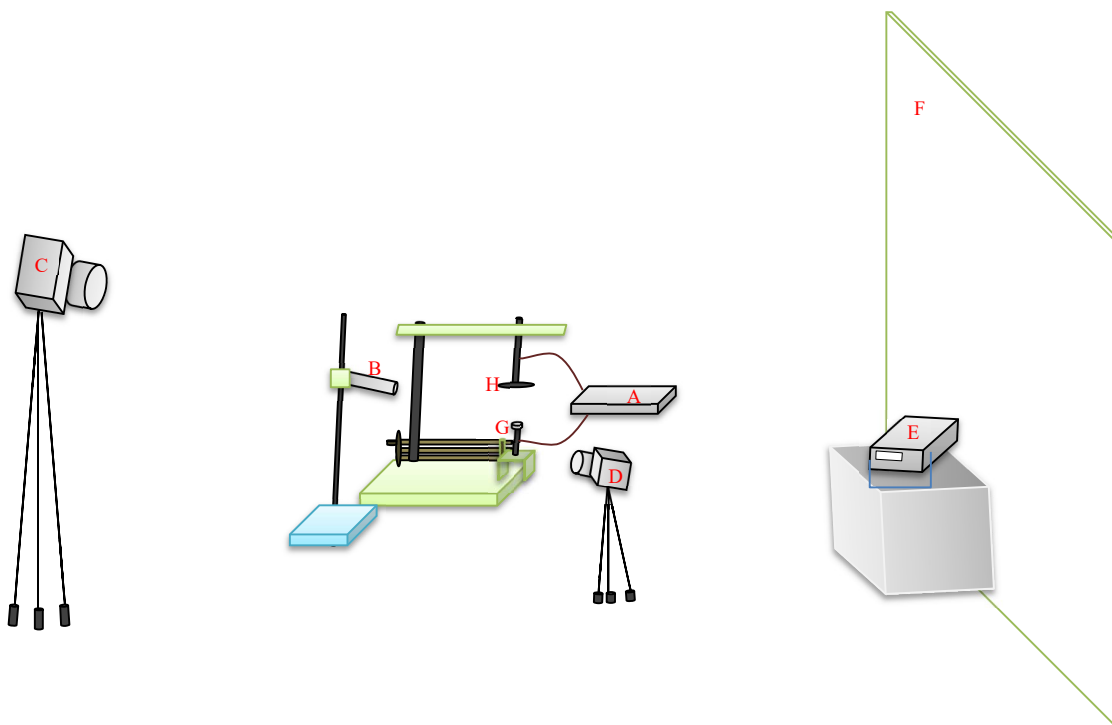


Figure 18. Experimental setup: A) Exciter; B) Laser; C) DSLR; D) UV Camera; E) Multimeter; F) Projection screen; G) Metallic container for polymer solution; H) Collector

3.1.1. Material details used in the setup

Following equipments and appliances were utilized in this experimental setup:

- a) HV source Matsusada AU series
- b) Green laser with wavelength of 532nm, output power of 100mW and working voltage of DC3.7V with cylindrical lens
- c) Nikon D3400 Digital single-lens reflex camera with Sigma 150mm f/2.8 EX DG HSM APO Macro Lens
- d) UV Camera CoroCam1
- e) Agilent 53131A multimeter
- f) Projection screen
- g) Metallic container for polymer solution with orifice diameter 3.685 cm and depth 1 cm.
- h) Collector
- i) DC electrospinning set up
- j) Polymer solutions
- k) Convex mirror for conducting characteristic experiment

Figure 19 shows the DC electrospinning set up with laser and the diffraction pattern on the screen.

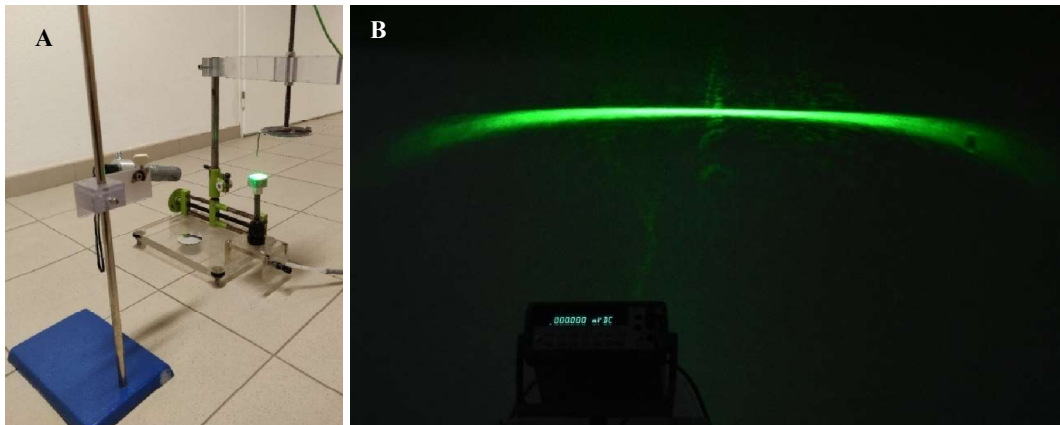


Figure 19. A) DC electrospinning set up with incident laser beam; B) Surface of water without applied voltage on the projection wall

3.2. Characteristic Experiment method

To determine the optimal positioning of each device utilized, a characteristic experiment was conducted employing a convex mirror characterized by significant curvature.

During the experimentation involving polymer solutions, the orifice die was filled beyond its capacity, leading to the formation of a convex meniscus. Consequently, a convex mirror was employed to replicate the system in the characteristic experiment.

Figure 20 depicts the experimental set up.

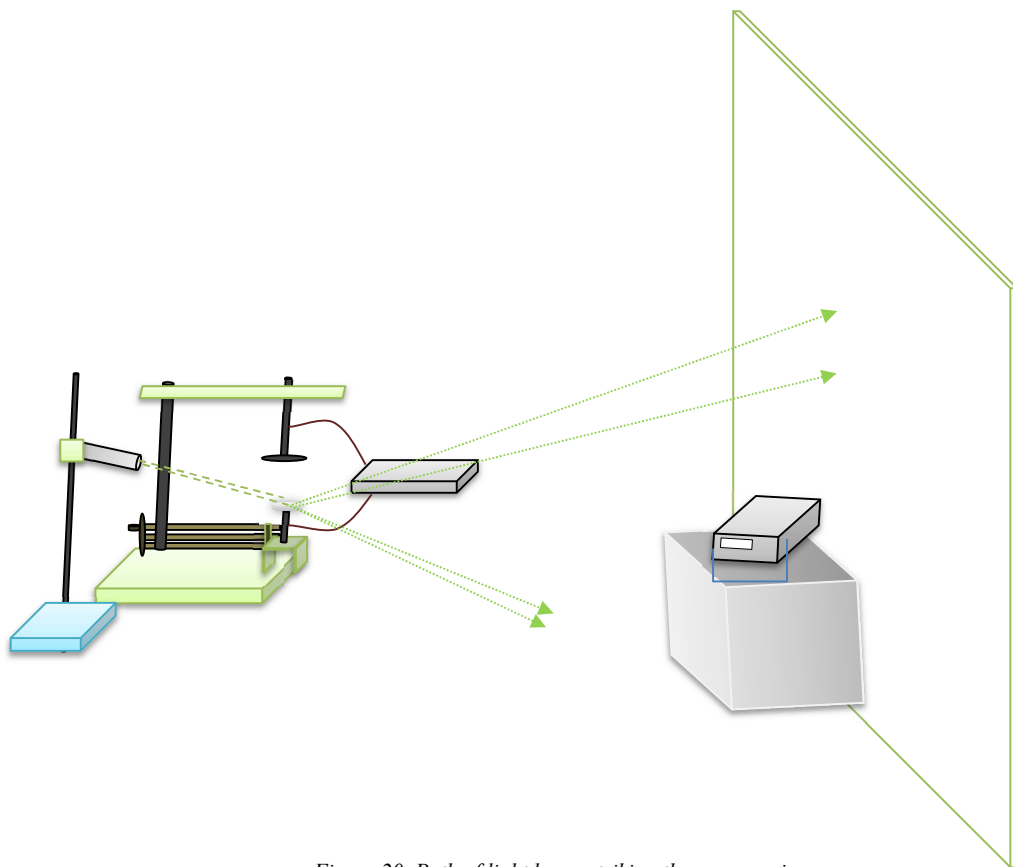


Figure 20. Path of light beam striking the convex mirror

The incident laser beam was directed at an angle ranging between 30 to 45 degrees. Additionally, the distances between the DC electrospinning apparatus and laser, and both the projection screen and DSLR camera were consistently maintained at 6.7 meters and 10 meters, respectively, throughout this experiment.

Figures 21 and 22 offer a comprehensive overview of the characteristic method that has been developed utilizing a mirror.

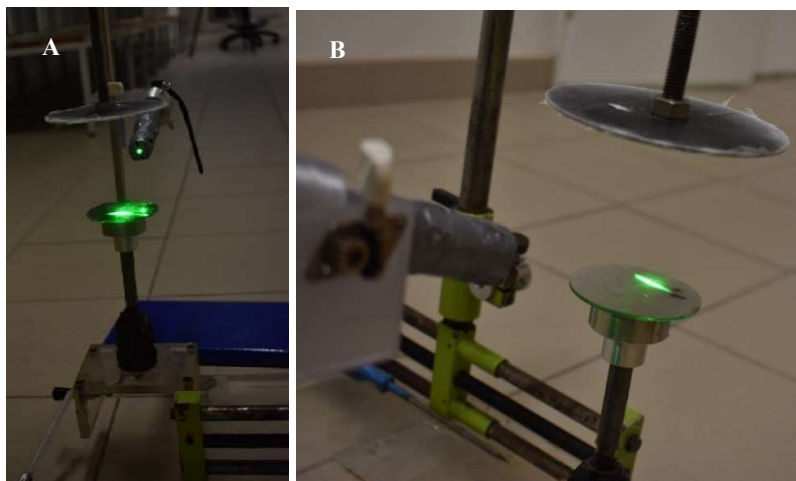


Figure 21. A) Front view B) Back view of laser beam on convex mirror

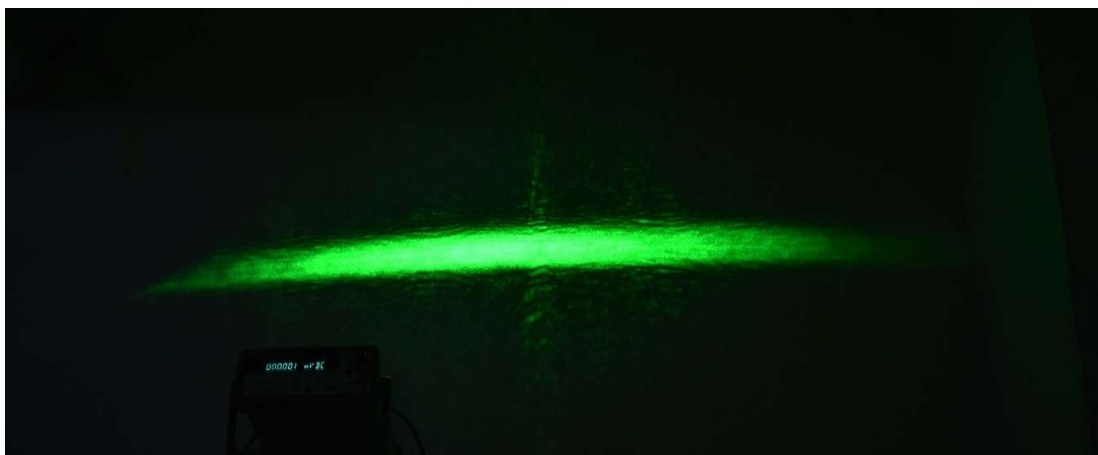


Figure 22. Diffraction pattern of mirror on the screen

The precise positioning achieved in the initial characteristic experiment was employed for subsequent experiments aimed at measuring surface records of all the polymer solutions. The following sections elucidate the details of the surface phenomena observed under applied voltage conditions for PVA in water and PVB in ethanol.

3.3. Behavior of polymer solution and self organisation of jets in applied voltage

The phenomenon of self-organization of jets on the free liquid surface is observed and is illustrated in Figure 23. The experimental setup involved depositing the polymer solutions into a metallic orifice with a diameter of 3.685 cm placed on metallic rod serving as an electrode, while a collector was positioned above it. In the absence of an applied voltage or electrostatic field, the solutions initially exhibited an approximately hemispherical shape as shown in Figure 23. (A). Upon activating a high voltage source to create an electrostatic field between the electrode and the collector, the shape of the solutions undergo a transformation. The outer surface of the solutions acquire net charges of the same sign, resulting in mutual repulsion through electrostatic forces. At this stage, the system's free energy minimizes by concentrating the net charges predominantly on the periphery of the solutions. Attractive Coulombic forces between the net charge on the periphery and the collector cause the formation of a swelling droplet rim, giving rise to a plate-like shape. As the strength of the applied field increased further, a significant feature described in the theoretical framework (as mentioned in the introduction of section 2.7) of the phenomenon emerged: a stationary wave organizes on the previously smooth rim. With even higher field intensities, jets simultaneously emerged from the crests of the stationary wave as illustrated in Figure 23. (B) and (C).

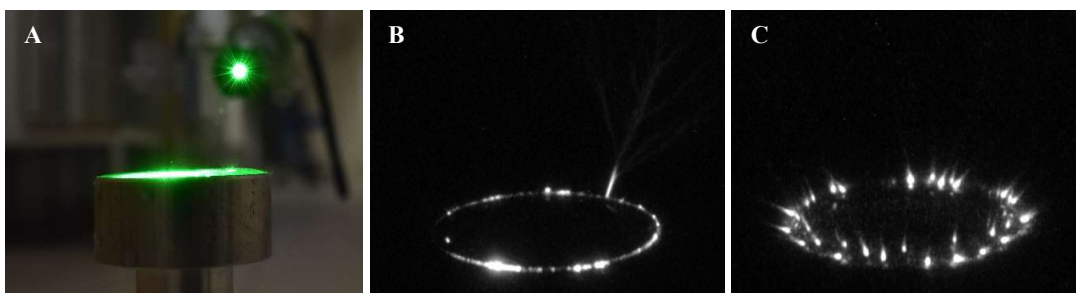


Figure 23. PVA solution with 10% concentration A) without applied voltage exhibiting a hemispherical/convex shape; B) and C) with voltage showing emerging jets, images captured under UV camera.

3.4. Data processing method

In this experiment, a video is recorded for each polymer solution, and the footage was projected onto a screen (in this case, a wall) using a laser. The captured frames had an aspect ratio of 16:9 and a resolution of 1920x1080 pixels. The surface observed on the screen is magnified approximately 50 times.

To measure the actual surface fluctuations, the readings obtained from the video frames were converted from pixels to millimeters. The high voltage source used in the experiment was manually operated. For each incremental voltage unit, an image frame was extracted using MATLAB image analysis toolbox, and the collective amplitude of the illuminated area in the diffraction pattern was measured.

Figure 24. shows the MATLAB function used for extraction of frames.

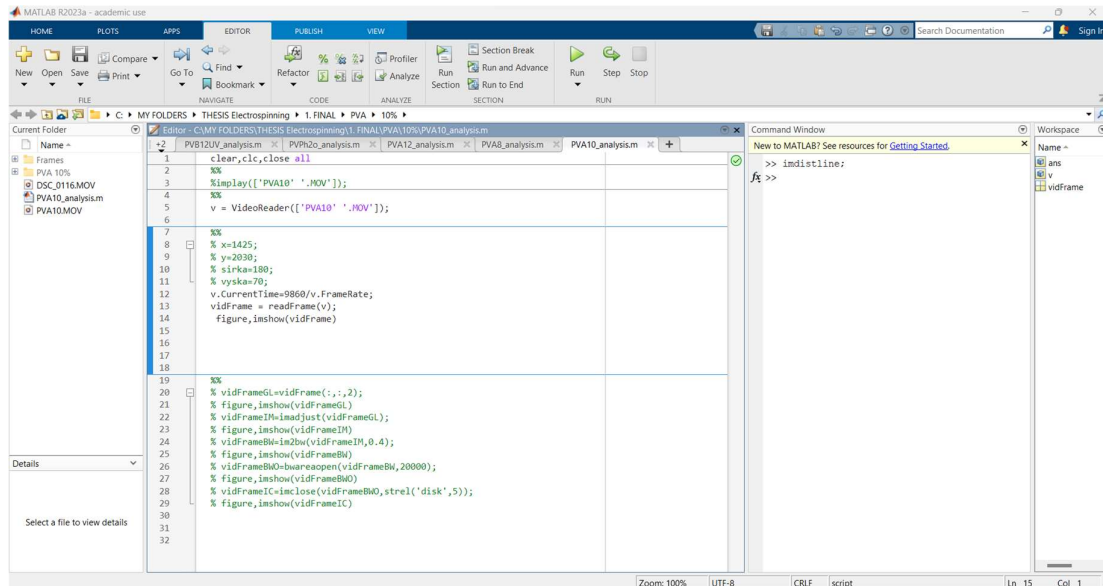


Figure 24. MATLAB screen

The applied voltage is represented by the symbol as V or φ (in kilovolts, kV), electrical intensity is denoted as E , while the measured fluctuation, hypothesized as the amplitude of collective waves, is denoted by d (in millimeters, mm).

Figure 25. Diffraction pattern observed in PVA 10% without applied voltage and at critical voltage(first corona discharge).

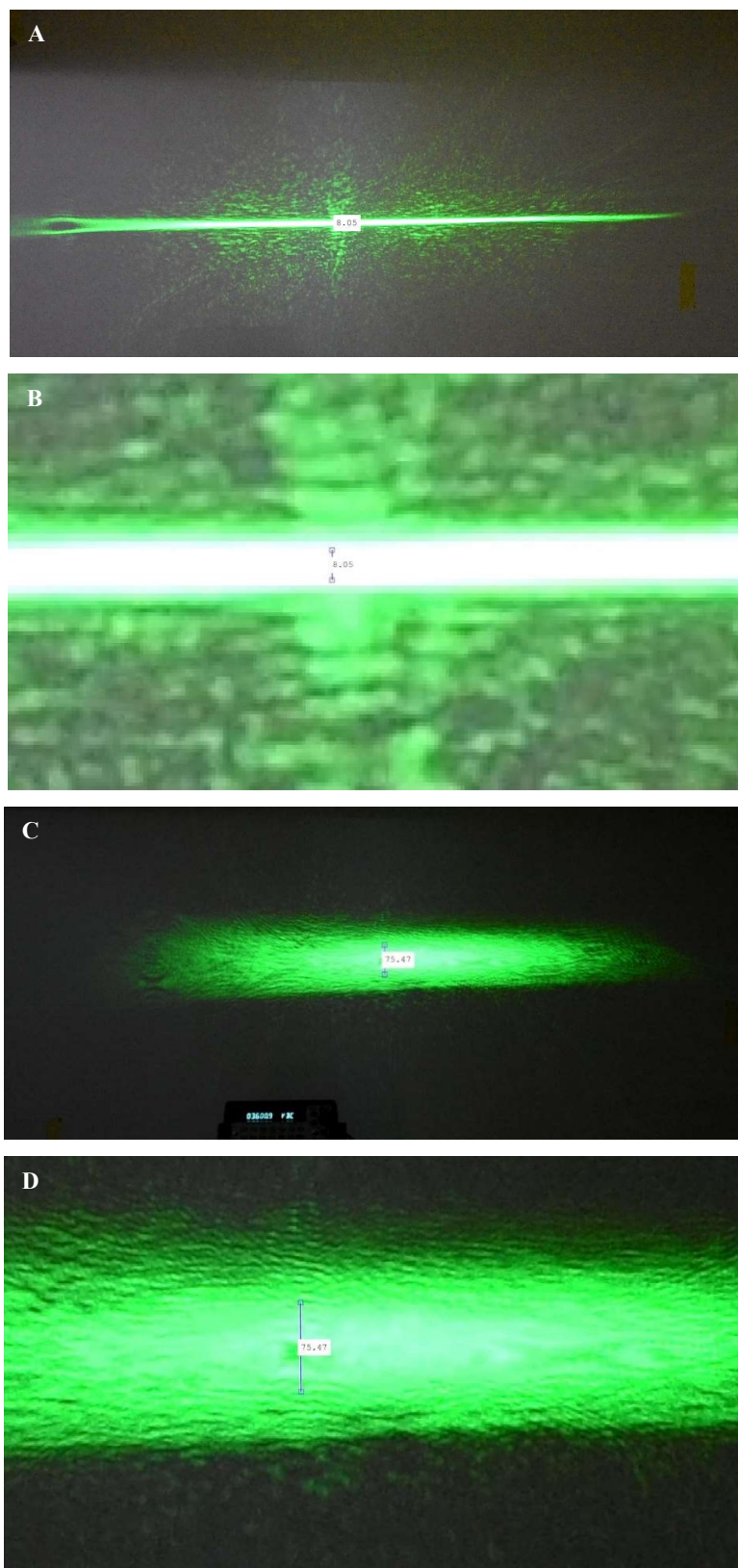


Figure 25. Measured illuminated height(d) in pixels. A and B without voltage, C and D at appearance of first corona discharge, with B and D showing the zoomed in images of A and B respectively

3.4.1. Experiment with Water and Ethanol

After the charcetrstic method, experiments are done on the solvents water and Ethanol.

Figure 26 illustrates the surface wave propogations observed for Water.

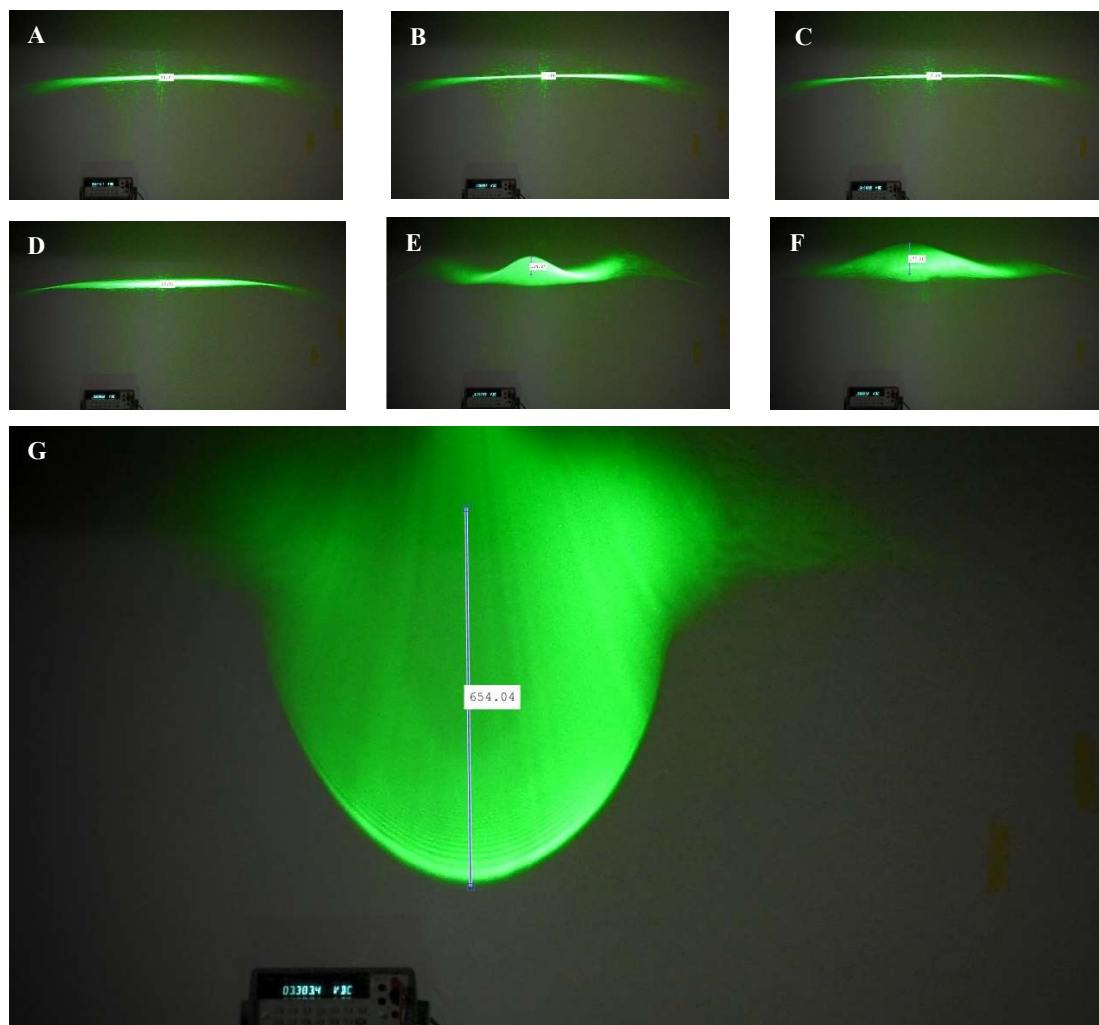


Figure 26. Diffraction pattern on surface of Water showing the surface wave propogations at A)5, B)10, C)15, D)20, E)25, F)30, and G)33.8(onset of jets) kV of applied voltage.

Figure 27, illustrates the surface wave propagations observed for Ethanol.

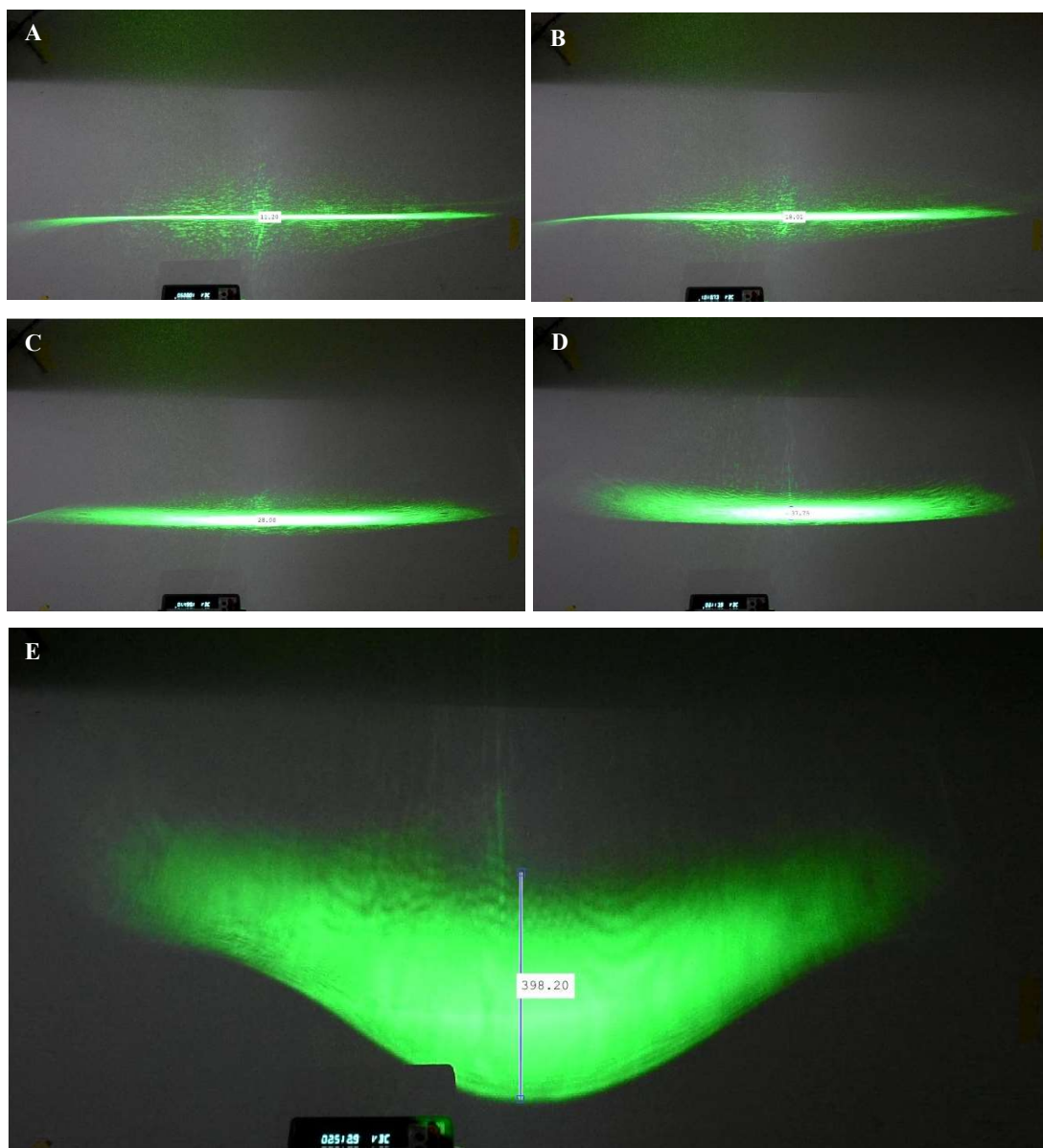


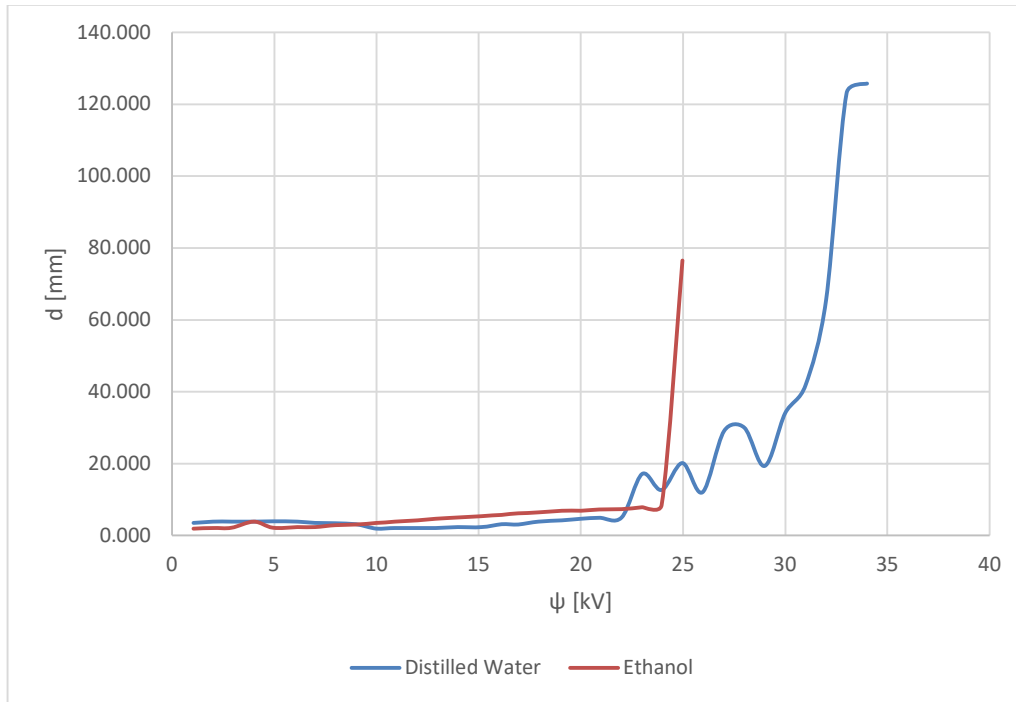
Figure 27. Diffraction pattern on the surface of Ethanol showing the surface wave propagations at A)5, B)10, C)15, D)21, and E)25(onset of jets) kV of applied voltage.

Table . 3. presents the measured values of fluctuation/amplitude observed at each unitary voltage value for Water and Ethanol.

Table 3. Observed measurements converted in mm for each unit voltage value

| φ [kV] | Distilled Water | Denatured Ethanol |
|----------------|-----------------|-------------------|
| | d [mm] | |
| 1 | 3.462 | 1.929 |
| 2 | 3.846 | 2.110 |
| 3 | 3.846 | 2.137 |
| 4 | 3.846 | 3.840 |
| 5 | 3.908 | 2.154 |
| 6 | 3.875 | 2.308 |
| 7 | 3.485 | 2.365 |
| 8 | 3.423 | 2.885 |
| 9 | 3.104 | 3.077 |
| 10 | 1.940 | 3.462 |
| 11 | 2.092 | 3.846 |
| 12 | 2.079 | 4.231 |
| 13 | 2.112 | 4.615 |
| 14 | 2.312 | 5.017 |
| 15 | 2.325 | 5.385 |
| 16 | 3.106 | 5.769 |
| 17 | 3.079 | 6.154 |
| 18 | 3.852 | 6.413 |
| 19 | 4.231 | 6.923 |
| 20 | 4.623 | 6.923 |
| 21 | 4.956 | 7.260 |
| 22 | 5.046 | 7.358 |
| 23 | 17.098 | 7.885 |
| 24 | 12.644 | 8.462 |
| 25 | 20.167 | 76.538 |
| 26 | 12.021 | |
| 27 | 29.073 | |
| 28 | 30.075 | |
| 29 | 19.319 | |
| 30 | 34.092 | |
| 31 | 41.923 | |
| 32 | 65.577 | |
| 33 | 123.077 | |
| 34 | 125.769 | |

Graph. 2. shows the dependence of measured propagation d [mm] to φ [kV] for Water and Ethanol.



Graph 2. Measurements with Water and Ethanol

3.4.2. Experiment with PVA in Water

Surface of polymer solution of PVA with mass concentration of 8%, 10% and 12% were observed under laser.

Table 4 presents the diffraction pattern observed for PVA at the onset of the first corona discharge. This indicates that at this particular point, the electric pressure is approximately equivalent to the capillary pressure.

Table 4. Surface phenomenon observed during the initial appearance of corona discharge in PVA


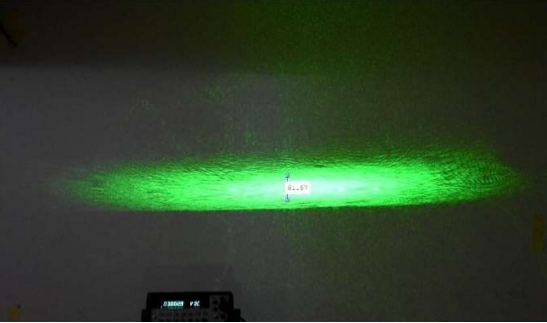




| | 1 st Corona discharge observed using UV camera | Diffraction pattern observed when 1 st discharge appears |
|------------|---|--|
| PVA 8% |  |  |
| PVA 10% |  |  |
| PVA 12% |  |  |

Table 5 presents the measured values of fluctuation/amplitude observed at each unitary voltage value.

Table 5. Observed measurements converted in mm for each unit voltage value

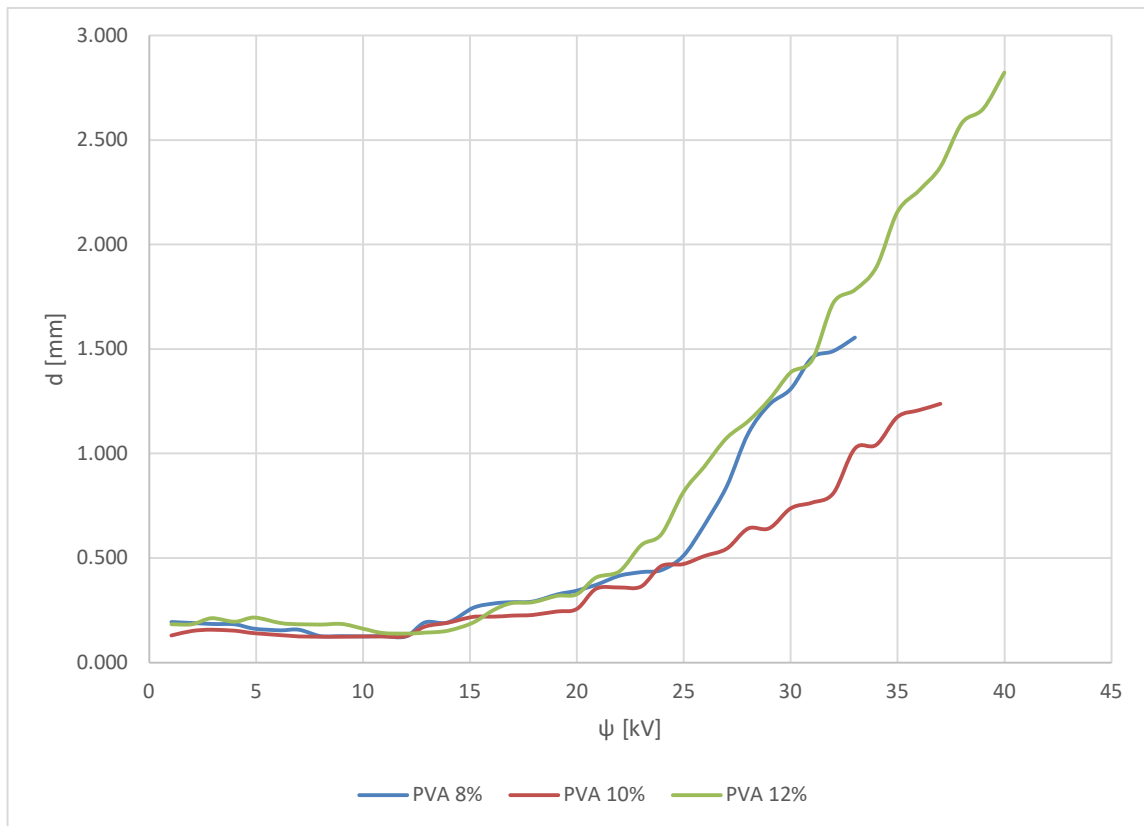
| | 8% | 10% | 12% |
|-------------|--------|-------|-------|
| ψ [kV] | d [mm] | | |
| 0 | 0.159 | 0.129 | 0.181 |
| 1 | 0.194 | 0.130 | 0.183 |
| 2 | 0.189 | 0.151 | 0.184 |
| 3 | 0.185 | 0.157 | 0.212 |
| 4 | 0.183 | 0.152 | 0.196 |
| 5 | 0.162 | 0.141 | 0.216 |
| 6 | 0.155 | 0.132 | 0.189 |
| 7 | 0.158 | 0.126 | 0.184 |
| 8 | 0.127 | 0.124 | 0.182 |
| 9 | 0.127 | 0.124 | 0.185 |
| 10 | 0.125 | 0.125 | 0.163 |
| 11 | 0.126 | 0.125 | 0.141 |
| 12 | 0.126 | 0.126 | 0.139 |
| 13 | 0.192 | 0.173 | 0.143 |
| 14 | 0.192 | 0.192 | 0.153 |
| 15 | 0.261 | 0.218 | 0.192 |
| 16 | 0.283 | 0.219 | 0.252 |
| 17 | 0.288 | 0.224 | 0.285 |
| 18 | 0.293 | 0.229 | 0.289 |
| 19 | 0.326 | 0.244 | 0.319 |
| 20 | 0.345 | 0.256 | 0.327 |
| 21 | 0.372 | 0.353 | 0.406 |
| 22 | 0.416 | 0.360 | 0.438 |
| 23 | 0.432 | 0.364 | 0.561 |
| 24 | 0.442 | 0.462 | 0.614 |
| 25 | 0.509 | 0.471 | 0.813 |
| 26 | 0.657 | 0.509 | 0.937 |
| 27 | 0.842 | 0.545 | 1.074 |
| 28 | 1.093 | 0.641 | 1.154 |
| 29 | 1.234 | 0.642 | 1.258 |
| 30 | | 0.738 | 1.388 |
| 31 | | 0.765 | 1.446 |
| 32 | | 0.811 | 1.721 |
| 33 | | 1.024 | 1.783 |
| 34 | | 1.042 | 1.891 |
| 35 | | 1.175 | 2.156 |
| 36 | | 1.207 | 2.258 |
| 37 | | 1.238 | 2.370 |
| 38 | | | 2.580 |
| 39 | | | 2.649 |
| 40 | | | 2.823 |

Table. 6. shows the correlation obtained between the applied voltage[kV] and observed value of d[mm].

Table 6. Correlation values between applied voltage[kV] and d[mm]

| PVA | Pearson Correlation(r) | Coefficient of determination(r ²) |
|-----|------------------------|---|
| 8% | 0.844 | 0.712 |
| 10% | 0.903 | 0.816 |
| 12% | 0.902 | 0.814 |

Graph. 3. shows the relation between ϕ [kV] and d[mm] for PVB with concentration 8%, 10%, 12%.



Graph 3. Measurements with PVA

3.4.3. Experiment with PVB in Ethanol

Another measurement was carried out for PVB with mass concentration of 8%, 10% and 12%.

The occurrence of the first corona discharge was observed at applied voltages of 28 kV, 26 kV, and 32 kV for mass concentrations of 8%, 10%, and 12%, respectively.

Table 7 presents the diffraction pattern observed at the onset of the first corona discharge.

Table 7. Surface phenomenon observed during the initial appearance of corona discharge.




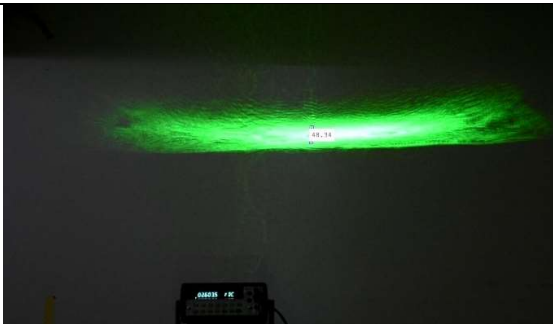


| | 1 st Corona discharge observed using UV camera | Diffraction pattern observed when 1 st discharge appears |
|------------|---|--|
| PVB 8% |  |  |
| PVB 10% |  |  |
| PVB 12% |  |  |

Table 8 presents the measured values of fluctuation/amplitude observed at each unitary voltage value.

Table 8. Observed measurements converted in mm for each unit voltage value

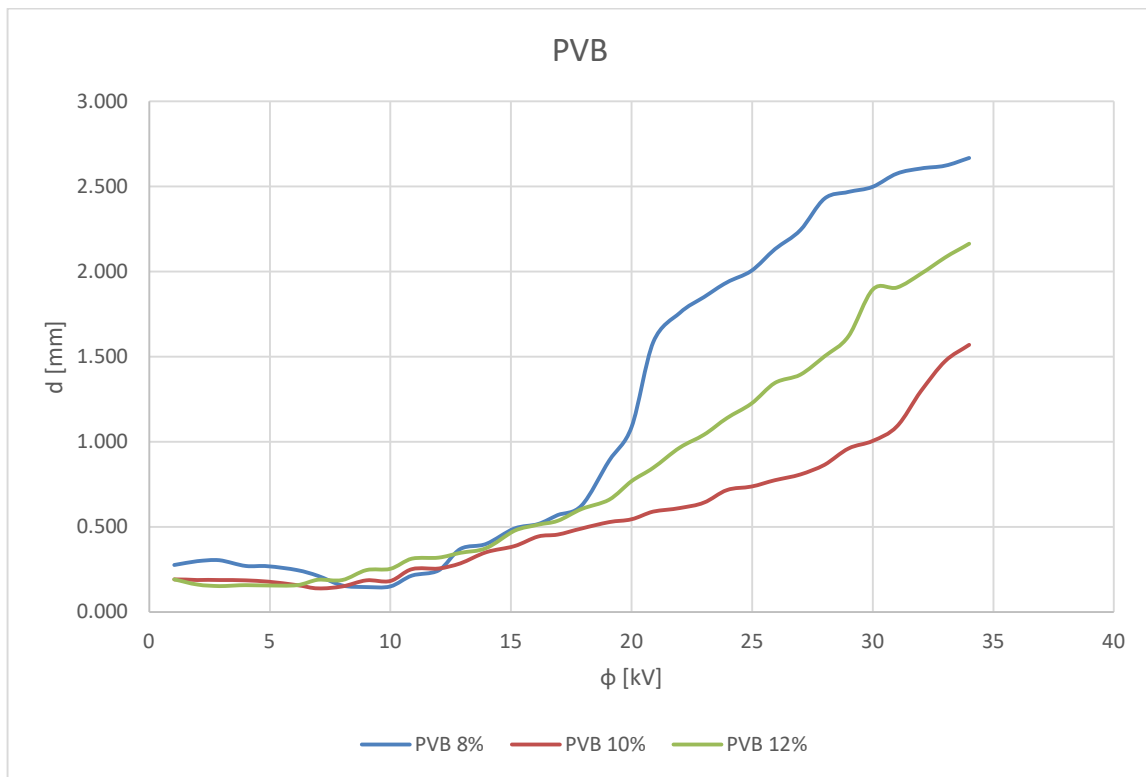
| φ [kV] | 8% | 10% | 12% |
|----------------|--------|-------|-------|
| | d [mm] | | |
| 1 | 0.277 | 0.192 | 0.192 |
| 2 | 0.299 | 0.189 | 0.162 |
| 3 | 0.304 | 0.189 | 0.153 |
| 4 | 0.271 | 0.186 | 0.158 |
| 5 | 0.270 | 0.178 | 0.156 |
| 6 | 0.247 | 0.158 | 0.158 |
| 7 | 0.213 | 0.139 | 0.189 |
| 8 | 0.156 | 0.151 | 0.188 |
| 9 | 0.147 | 0.186 | 0.247 |
| 10 | 0.151 | 0.183 | 0.255 |
| 11 | 0.215 | 0.253 | 0.314 |
| 12 | 0.245 | 0.255 | 0.320 |
| 13 | 0.370 | 0.287 | 0.347 |
| 14 | 0.401 | 0.353 | 0.376 |
| 15 | 0.491 | 0.388 | 0.477 |
| 16 | 0.517 | 0.443 | 0.513 |
| 17 | 0.569 | 0.455 | 0.536 |
| 18 | 0.626 | 0.491 | 0.605 |
| 19 | 0.890 | 0.529 | 0.661 |
| 20 | 1.087 | 0.545 | 0.769 |
| 21 | 1.586 | 0.590 | 0.848 |
| 22 | 1.758 | 0.612 | 0.967 |
| 23 | 1.851 | 0.643 | 1.042 |
| 24 | 1.937 | 0.717 | 1.139 |
| 25 | 2.005 | 0.737 | 1.225 |
| 26 | 2.132 | 0.775 | 1.346 |
| 27 | 2.244 | 0.809 | 1.396 |
| 28 | 2.429 | 0.865 | 1.503 |
| 29 | 2.468 | 0.962 | 1.621 |
| 30 | 2.499 | 1.006 | 1.896 |
| 31 | 2.576 | 1.090 | 1.907 |
| 32 | 2.607 | 1.298 | 1.987 |
| 33 | 2.622 | 1.474 | 2.083 |
| 34 | 2.668 | 1.571 | 2.163 |

Table. 9. shows the correlation obtained between the applied voltage[kV] and observed value of d[mm].

Table 9. Correlation values between applied voltage[kV] and d[mm] for PVB

| PVB | Pearson Correlation(r) | Coefficient of determination(r^2) |
|-----|------------------------|---------------------------------------|
| 8% | 0.922 | 0.850 |
| 10% | 0.959 | 0.920 |
| 12% | 0.987 | 0.974 |

Graph. 3. shows the realltion between ϕ [kV] and d[mm] for PVB with concentration 8%, 10%, 12%.



Graph 4. Measurements with PVB

4. Results and Discussion

Based on the observed fluctuations in measurements, it has been observed that the polymer solutions initially forms a thick layer upon applying voltage up to 4-7 kV. Subsequently, between 7-10 kV, the surface starts to thin out, but it thickens again until nanofibers are generated. The voltage required for these changes depends on the specific polymer solutions and their mass concentrations.

Based on empirical observations, it is hypothesized that the initial phenomenon of surface layer thinning can be attributed to the prevailing influence of capillary pressure over electrostatic pressure. Through the investigation of the Pearson correlation between the thickening of the surface layer(from 11 kV) and the occurrence of the first corona discharge(between 26-37kV depending the mass concentration of polymer solution), a strong linear relationship is revealed. This relationship is governed by the second-order electrical intensity (E^2), which is directly proportional to the second order of the applied voltage/electrostatic potential (φ^2), as well as the measured amplitude (d) in millimeters. These findings are consistent with established scientific principles concerning the interplay between electrostatic potential and electrical intensity. Equation 6 in section 2.5.1 states that the electrical field intensity (E) can be obtained by taking the gradient of the electric potential (V) at a specific point, with a change of sign:

$$E = - \nabla V$$

Furthermore, since V is directly proportional to E, we can express it as:

$$V^2 \propto E^2$$

In the context of this experiment, the applied voltage (V) can be considered as a proportional value for E. Therefore, when analyzing the values of d (amplitude in millimeters) and V^2 for each polymer solution, a correlation can be established, ultimately providing insights into the relationship with electric pressure. Electric pressure is defined as $\frac{1}{2} \epsilon E^2$, where ϵ is a constant.

4.1. Behavior of Water and Ethanol under Applied Voltage

Section 2.7 of the study discusses the phenomenon known as self-organization of jets in electrospinning. This phenomenon, also referred to as Plateau-Rayleigh instability, occurs when the fastest forming instability leads to the spontaneous formation of jets. Observations conducted with Water and Ethanol confirm the occurrence of this behavior. The parameter "d" exhibits a significant increase at 33kV and 25kV for Water and Ethanol, respectively. This observation provides further evidence supporting the theory of self-organization of jets.

Another notable finding is that the values of "d" in Ethanol are initially as well as at the onset of jets formation are consistently lower for each unitary voltage value. This behavior can be explained by considering the damping coefficient, which is determined by the equation:

$$\gamma = 2\eta \frac{\omega^4}{g^2}$$

where, γ is the damping coefficient, η is then kinematic viscosity, ω is the angular frequency and g is the gravitational acceleration.

In the experiment, the wavelength (λ) depends on the illuminated line on the orifice, which corresponds to the orifice diameter (3.685 cm). The angular frequency can be calculated using the formula $\omega = 2\pi/\lambda$. To determine the damping coefficient for Water and Ethanol in this experiment, the only variable is the kinematic viscosity (η). Using the values of η , ($1.004 \cdot 10^{-6}$ for water and $1.074 \cdot 10^{-6}$ for ethanol), λ (3.685 cm), and g (9.834 m/s^2) provided, the angular frequency (ω) is calculated to be 170.50/m.

The calculated, damping coefficient for both the solvents are:

$$\gamma_{\text{water}} = 17.55 /s$$

$$\gamma_{\text{ethanol}} = 18.77 /s$$

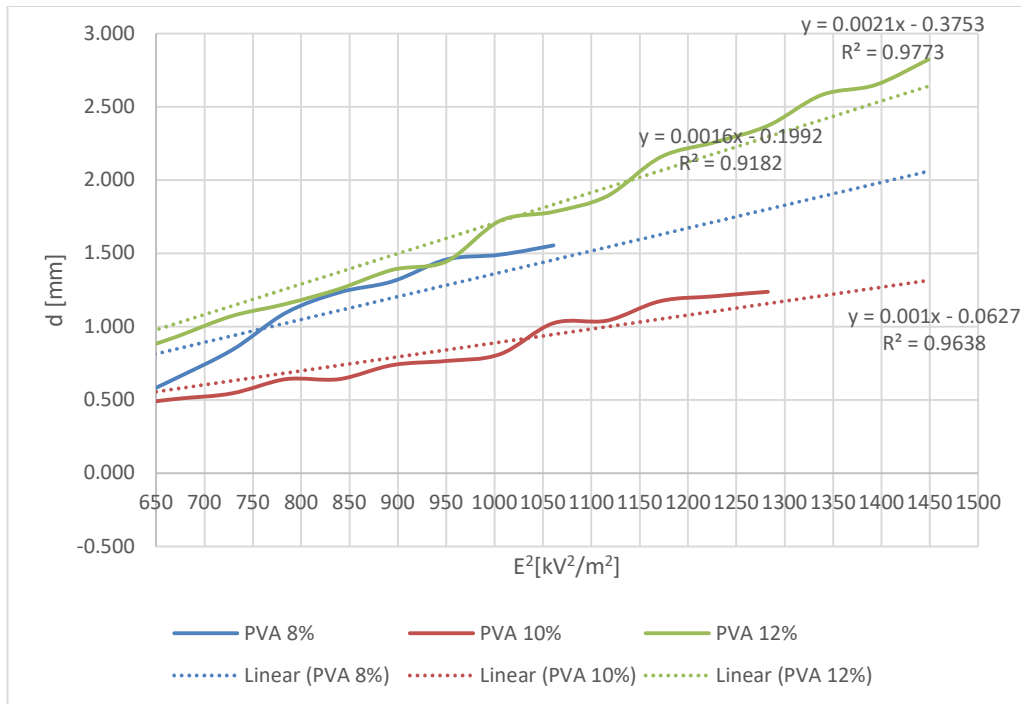
These results offer insights into the suppression of waves occurring in Ethanol during the experiment.

4.2. Mathematical parametric correlation in PVA

Graph. 5. showcases the coefficient of determination between the second order of electrical intensity (E^2) and the amplitude (d) for PVA. The data points are collected within the voltage range of 11 kV (corresponding to the thickening) up to 37 kV (corresponding to the onset of the first corona discharge).

Table 10. Correlation values between Electrical intensity [kV^2/m^2] and d [mm] for PVA

| PVA | Pearson Correlation(r) | Coefficient of determination(r^2) |
|-----|------------------------|---------------------------------------|
| 8% | 0.923 | 0.9182 |
| 10% | 0.981 | 0.9631 |
| 12% | 0.984 | 0.9680 |



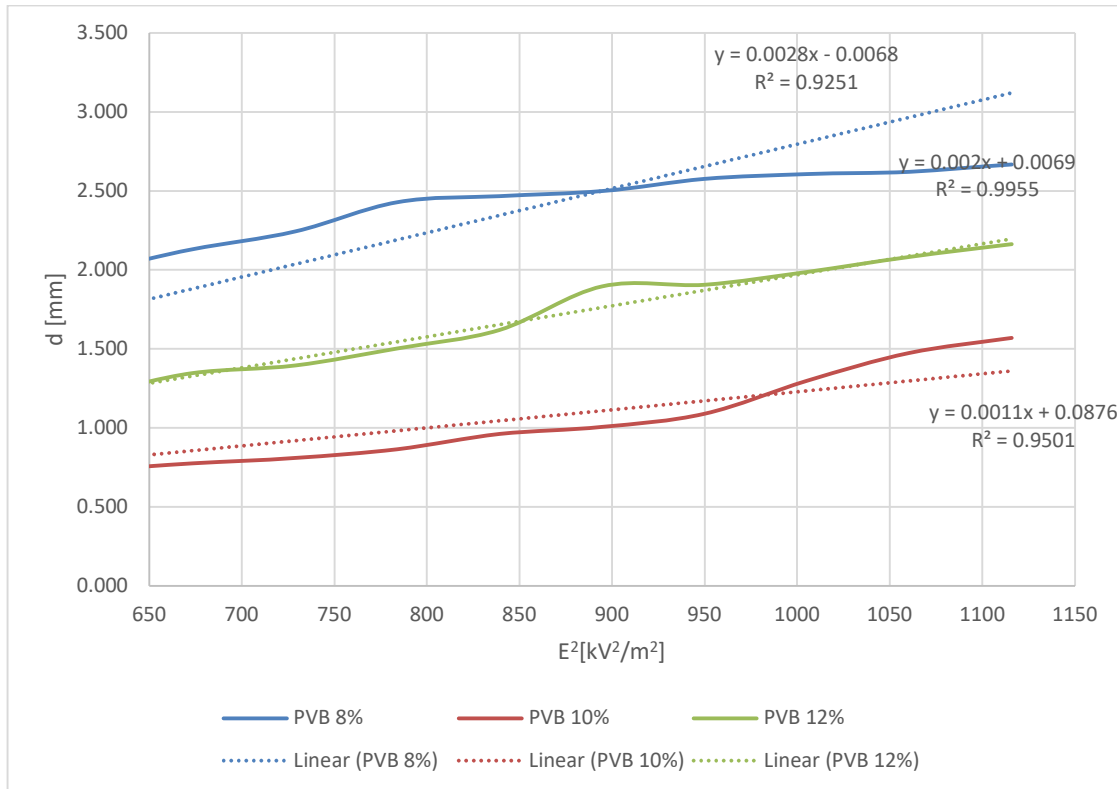
Graph 5. Dependence of d [mm] on E^2 [kV^2/m^2] for PVA

4.3. Mathematical parametric correlation in PVB

Graph. 5. showcases the coefficient of determination between the second order of electrical intensity (E^2) and the amplitude (d) for PVB. The data points are collected within the voltage range of 11 kV (corresponding to the onset of the first corona discharge) up to 34 kV, specifically focusing on PVB with a mass concentration of 10%.

Table 11. Correlation values between Electrical intensity [kV^2/m^2] and d [mm] for PVB

| PVB | Pearson Correlation(r) | Coefficient of determination(r^2) |
|-----|------------------------|---------------------------------------|
| 8% | 0.962 | 0.925 |
| 10% | 0.975 | 0.950 |
| 12% | 0.998 | 0.996 |



Graph 6. Dependence of d [mm] on E^2 [kV^2/m^2] for PVB

5. Conclusion

This thesis aims to conduct a comprehensive literature review on surface waves and their relationship to electrospinning. Additionally, it focuses on the construction of an experimental setup to evaluate surface phenomena during direct current (DC) electrospinning.

The capillary wave profile technique is employed based on the findings from the literature review. This technique utilizes a laser to create a magnified diffraction pattern, enabling the detection of surface waves on various polymer solutions with different concentrations. To capture visual representations of these patterns, DSLR and UV cameras are utilized.

The constructed experimental setup allows for an approximate fifty-fold magnification of the surface phenomenon. The observations indicate that the diffraction pattern undergoes an initial thickening, followed by thinning, and then continues to thicken until nanofibers are formed. Based on these observations, a hypothesis is proposed, suggesting that the initial thinning occurs due to capillary pressure surpassing electrostatic pressure. Through the evaluation of values from the onset of layer thickening until the first corona discharge, a robust correlation is identified between wave propagation and electric pressure. This correlation is hypothesized to be attributed to the amplitude of interference.

However, the analysis of the interference/fringing pattern or noise surrounding the illuminated diffraction pattern is lacking in this study. To delve deeper into the analysis of the diffraction pattern, it is suggested to investigate the application of Speckle interferometry.

Overall, this thesis work endeavors to provide a comprehensive literature review on surface waves and their relation to electrospinning. Furthermore, it aims to construct an experimental setup for evaluating surface phenomena during DC electrospinning, utilizing the capillary wave profile technique and considering the potential application of Speckle interferometry for further analysis of the diffraction pattern.

6. Experiment limitations and suggestions

The experimental setup employed in this study exhibits a significant constraint when it comes to automated data generation. In order to acquire the desired data, a manual procedure was implemented, wherein each frame was individually extracted for every unitary voltage value, followed by a manual measurement of the illuminated width hypothesized as amplitude. Consequently, a discrete set of values was obtained. This manual approach was necessitated due to the presence of lens flare in the captured videos, which obstructed the optical character reading in MATLAB required for extracting the voltage values from the multimeter.

To address the above challenge, potential solutions can be explored. One approach involves utilizing a separate camera specifically dedicated to capturing the values displayed on the multimeter. This would enable a more accurate and reliable extraction of the voltage data. Alternatively, employing a higher-power lens to capture more focused frames could also alleviate the issue of lens flare, facilitating improved readability and extraction of the voltage values. By implementing these measures, the limitations associated with the manual extraction of frames and amplitude measurement could be overcome, enhancing the efficiency and accuracy of the data generation process.

Another limitation arises from the characteristics of the high voltage source employed in the experiment. Owing to its inherent manufacturing properties, discernible fluctuations in the pattern only manifest during the turning of the knob. By gradually increasing the applied voltage through knob manipulation, wave fluctuations occur, followed by a subsequent settling of the waves. Nonetheless, it is worth noting that the extent of this settling phenomenon diminishes as the voltage approaches higher values.

References

- [1] S. P. S. S. Andrew S Ball, „Introduction into nanotechnology and microbiology,“ v *Methods in Microbiology*, Elsevier Ltd., 2019.
- [2] R. L. X. L. J. X. Shixuan Chen, „Electrospinning: An enabling nanotechnology platform for drug delivery and regenerative medicine,“ sv. 132, č. Advanced Drug Delivery Reviews on "3D-Bioprinting and Micro-/Nano-Technology: Emerging Technologies in Biomedical Sciences"., July 2018.
- [3] A. L. Y. Darrell H. Reneker, „Electrospinning jets and polymer nanofibers,“ sv. 49, č. 10, 2008.
- [4] „Electrospinning of Polymer Nanofibers with Ordered Patterns and Architectures,“ sv. 10, č. Journal of Nanoscience and Nanotechnology, 2010.
- [5] G. O. J. T. M. a. Y. X. Dan Li, „Collecting Electrospun Nanofibers with patterned electrodes,“ sv. 5, 2005.
- [6] L. J. W. X. Q. W. Xu Lei, „Wave propagation of bending jet in electrospinning process,“ sv. 13, č. 4, 2023.
- [7] H. R. K. H. J. J. S. M. P. S. Nick Tucker, „The History of the Science and Technology of Electrospinning from 1600 to 1995,“ č. Special Issue- July 2012- Fibers, 2012.
- [8] D. Lukas, „Nanovlakna Teorie, technologie a pouziti,“ 2021.
- [9] A. I. G. a. S. O. Shir'aeva, „Mechanism of electrostatic polydispersion of liquid,“ sv. 23, č. 11, 1990.
- [10] K. F. W.-E. T. T.-C. L. Z. M. Seeram Ramakrishna, An Introduction to Electrospinning and Nanofibers, World Scientific Publishing Co. Pte. Ltd., 2005.
- [11] A. Ram, Fundamentals of Polymer Engineering, New York: Springer Science+Business Media , 1997.
- [12] J. D. a. D. H. Reneker, „Electrospinning Process and Applications of Electrospun fibers,“ sv. 35, č. 2-3, 1995.
- [13] A. H. K. S. D. K. E.-j. K. I. K. Hyun-Su Bae, „Fabrication of highly porous PMMA electrospun fibers and their application in the removal of phenol and iodine,“ 2013.
- [14] R. Feynman, „Chapter 41 The Flow of Wet Water,“ v *The Feynman Lectures of Physics Volume II*, Addison-Wesley Publishing Company, 1963.

- [15] S. R. M. Yousefzadeh, „13- Modelling performance of electrospun nanofibers and nanofibrous assemblies,“ v *Electrospun Nanofibers*, Woodhead Publishing, 2016.
- [16] S. A. M. H. V. J. Tahere Mazoochi, „Investigation on the Morphological Characteristic of Nanofibrous Membrane as Electrospun in the Different Processing Parameters,“ 2012.
- [17] S. D. Lucy A. Bosworth, „Acetone, a Sustainable Solvent for Electrospinning Poly(ϵ -Caprolactone) Fibres: Effect of Varying Parameters and Solution Concentrations on Fibre Diameter,“ 2012.
- [18] C. X. M. K. S. R. X.M. Mo, „Electrospun P(LLA-CL) nanofiber: a biomimetic extracellular matrix for smooth muscle cell and endothelial cell proliferation,“ sv. 25, č. 10, 2004.
- [19] A. S. P. P. David Lukas, „Self organization of jets in electrospinning from free liquid surface,“ *Journal of Applied Physics*, 2008.
- [20] E. M. I. L. D. Landau, „Course of Theoretical Physics Volume 6,“ v *Fluid Mechanics 2nd edition*, Elsevier Ltd., 1987.
- [21] G. B. Whitham, *Linear and Nonlinear Waves*, New York: A Wiley-Interscience Publication JOHN WILEY & SONS, INC., 1999.
- [22] S. K. A. L. Yarin, „Bending Instability in Electrospinning of Nanofibers,“ sv. 89, 2001.
- [23] M. H. b. M. B. c. G. R. d. Y.M. Shin a, „Experimental characterization of electrospinning: the electrically forced jet and instabilities,“ sv. 42, č. 25, 2001.
- [24] B. S. L. R. H. M. K. Abdullah Khalil, „Electrospun metallic nanowires: Synthesis, characterization, and applications,“ sv. AIP Publishing LLC, 2013.
- [25] R. H. J. Adin Mann Jr., „Propagation characteristics of capillary ripples, III. Capillary ripple velocity and attenuation dispersion on clean water surfaces and on various monolayers,“ sv. 18, č. 9, 1963.
- [26] G. W. a. F. Garbay, „Light scattering by surface tension waves,“ sv. 47, č. 4, 1979.
- [27] „. B. P. A. S. I. Radomir I. Slavchov, „Characterization of capillary waves: a review and a optical method,“ sv. 33, č. 10, 2021.
- [28] J. C. E. a. R. C. McGivern, „Photon correlation spectroscopy of thermal fluctuations of liquid surfaces,“ Sv. %1 z %2Journal of Physics D: Applied Physics, Volume 20, , č. 1, 1986.
- [29] K. Mâlo/y, J. Feder a T. Jo/ssang, „An experimental technique for measurements of capillary waves,“ *Rev Sci Instrum* 60, 481–486 (1989), 1989.
- [30] J. Hecht, „A short history of Laser development,“ sv. 49, č. 25, 2010.

- [31] C. R. J. L. Satish Kumar Rajasekharan, „LED based real-time survival bioassays for nematode research,“ 2018.
- [32] P. K. Gupta, Laser Physics and Technology, Springer Proceedings in Physics 160, 2012.
- [33] „NIF's Guide to How Lasers Work,“ Lawrence Livermore National Security, LLC, [Online]. Available: <https://lasers.llnl.gov/education/how-lasers-work>.
- [34] M. M. E.-G. M. S. Z. Mohammad D. Al-Amri, Optics in our time, Springer Nature Switzerland AG., 2016.
- [35] J. T. I. H. V. P. J. S. & V. Š. O. Lyutakov, „Polymer surface patterning by laser scanning,“ 2013.
- [36] A. C. S. D. R. S. Emo Chiellini*, „Biodegradation of poly (vinyl alcohol) based materials,“ sv. 28, č. 6, 2003.
- [37] P. R. SUNDARARAJAN, „Poly(vinyl alcohol),“ v *Polymer Data Handbook*, Oxford University Press, Inc., 1999.
- [38] P. R. SUNDARARAJAN, „Poly(vinyl butyral),“ v *Polymer Data Handbook*, Oxford University Press, Inc., 1999.
- [39] T. V. Bazhenova, „Waves in fluids,“ 2010.
- [40] W. N. L.-M. Z. C. B.-W. Deng-Guang Yu, „Fast Dissolution Nanofiber Membrane of Ferulic Acid Prepared Using Electrospinning,“ 2010.